INTERNATIONAL COMPUTER SCIENCE INSTITUTE

1947 Center St. • Suite 600 • Berkeley, California 94704-1198 • (510) 643-9153 • FAX (510) 643-7684

SAR image segmentation exploiting no background knowledge on speckled radiance: A feasibility study

A. Baraldi* and F. Parmiggiani†

TR-98-018

June 1998

Abstract. This work presents a SAR image segmentation scheme consisting of a sequence of four modules, all selected from the literature. These modules are: i) a speckle model-free contour detector that is the core of the segmentation scheme; ii) a geometrical procedure to detect closed regions from non-connected contours; iii) a region growing procedure whose merging rules exploit *local image properties*, both topological and spectral, to eliminate artifacts and reduce oversegmentation introduced by the second stage; iv) a neural network clustering algorithm to detect *global image regularities* in the sequence of within-segment properties extracted from the partitioned image provided by the third stage. In the framework of a commercial image-processing software toolbox, the proposed SAR image segmentation scheme employs a contour detector that is promising because: i) it is easy to use, requiring the user to select only one contrast threshold as a relative number; and ii) it exploits no prior domain-specific knowledge about the data source and the content of the scene, i.e., it is capable of processing SAR images as well as both achromatic and multispectral optical images. The segmentation scheme is tested on three images acquired by different SAR sensors. The robustness of the segmentation method is assessed by changing only one parameter of the procedure in the different experiments. Experimental results are interpreted as an encouragement to focus further multidisciplinary research on how to combine responses of multi-scale filter banks in low-level visual systems.

Keywords: speckled radiance, speckle noise, image segmentation, low-level vision.

*ICSI, 1947 Center Street, Suite 600, Berkeley, CA 94704-1198, Ph.: +1+510+643-9153, Fx.: +1+510+643-7684, Email: baraldi@icsi.berkeley.edu

†IMGA-CNR, Via Gobetti 101, 40129 Bologna (Italy), Ph.: +39+51+639-8009; Fax: +39+51+639-8132, Email: parmi2@imga.bo.cnr.it

1 Introduction

In recent years, the scientific community has been involved in an important debate on the reasons why the many image processing techniques presented in the literature have had such slight impact on their potential field of application [1]-[4]. To take this debate into account, we have attempted to make this paper as "focused on its very original core" as possible [4]. This original core is regarded as a set of useful items that a broad scientific audience would like to include in commercial image-processing all-purpose software toolboxes [4].

In the coming era of coherent imaging systems, one of the major challenges the remote sensing community will have to cope with is the analysis of large volumes of SAR data where intrinsic scene texture (within-class variability) is overlaid by speckle texture, especially at the spatial resolution of spaceborn SAR systems [5]. It has been shown that SAR data segmentation is useful in classification [6]-[8], feature extraction [9] and change detection tasks [10]. Segmentation of SAR images is traditionally considered more difficult than segmentation of incoherent (optical) images. Since heuristic filters (block averaging, median, etc.) have proved inadequate in removing speckle noise [5], [11], intelligent incorporation of *a priori* (background) knowledge has become fundamental to provide end users with powerful SAR image processing tools [12]. In recent years, proposed speckled and unspeckled scene models [5], [11], [13]-[18], have been incorporated in adaptive speckle filters, speckle contour detectors and SAR image segmentation systems [6], [7], [9], [19], [20].

Our objective is to select from the literature an unsupervised SAR image segmentation procedure considered feasible (in terms of performance, robustness, computation time) for inclusion in a commercial image-processing toolbox whose goal is the extraction of geophysical information (texture, shape, size, orientation, etc.) from regions of the image that are perceived as pictorially uniform by a photointerpreter for classification purposes. The SAR image segmentation procedure must be unsupervised in the sense that it will segment SAR images without *a priori* knowledge of: i) the number of surface classes depicted in the image; and ii) the statistical properties characterizing each thematic class (e.g., n-th order statistics computed off-line from supervised training samples).

Our work starts by selecting from the literature what we consider the most relevant SAR image segmentation procedure. Experimental results show that segmented images generated with this procedure are oversegmented for classification tasks. To reduce oversegmentation, an alternative SAR image segmentation procedure consisting of processing blocks taken from the literature is proposed. Thus, we do not claim to present yet another picture segmentation algorithm [4].

This paper is organized as follows. Section 2 briefly overviews models of the speckled scene. Section 3 points out the relationship between adaptive speckle filters and speckle contour detectors. Section 4 discusses the state of the art in SAR image segmentation schemes. Section 5 proposes a general-purpose segmentation framework capable of processing SAR as well as optical monochromatic and multi-spectral images. In Section 6 implementation details are discussed, while experimental results are discussed in Section 7 and conclusions are presented in Section 8.

2 Background knowledge about speckled radiance

Every coherent imaging system, like the SAR, is affected by constructive and destructive interference of scatterers within a resolution cell. This interference generates light and dark pixels in the image from regions that are homogeneous on the ground: such a visual effect is known as speckle noise [19]. Typically, speckle noise is considered a multiplicative random process, which is tantamount to stating that it is supposed to be "fully developed" [13], [21]. The multiplicative speckle model holds true when: i) within each resolution cell there are many independent scatterers; and ii) these independent scatterers feature: a) the same backscatter coefficient (i.e., all scatterers belong to a homogeneous area); b) the backscatter coefficient and phase functions are independent; and c) phases are uniformly distributed in the range $[0, 2\pi]$ [13], [21]. The multiplicative speckle model loses its validity where speckle is partially developed. This condition occurs in each resolution cell where: i) few strong scatterers are present, e.g., in corner and specular reflectors; and ii) a large number of independent scatterers are present, but they feature different backscatter coefficients. The latter condition occurs where resolution cell size is larger than or comparable to the size of scene details, e.g., near/across image contours and within highly textured areas (consisting of small texels).

Based on ecological observations as well as experimental studies on SAR image textures [5], [14], [18], it is now well accepted that for a wide variety of scattering situations, such as homogeneous and textured terrain classes (including extended vegetated areas), the probability density function (pdf) of unspeckled (noise-free) radiance can be modeled by a Gamma distribution. When the "fully developed speckle" hypotheses hold true, then the Gamma-distributed (true) scene model is modulated by either an independent complex-Gaussian speckle model (in complex SAR images) or by a Gamma speckle model (in multilook detected SAR images). This product gives rise to a K-distributed speckled observed radiance [5], [11], [13]-[17].

3 Speckle filters depend on speckle contour detectors

The basic idea underlying the development of adaptive speckle filters is to exploit *a priori* fully developed speckle model flexibly, i.e., only where this model holds true, by computing local (adaptive) statistics on (adaptive) neighborhoods adjusted to cover homogeneous natural extended targets [14], [15], [22]-[26]. In other words, since the fully developed speckle hypotheses do not hold true across image boundaries (i.e., across non-homogeneous areas, see Section 2), it is clear that the difference between speckle filters and speckle contour detectors becomes subtle, as *adaptive speckle filters must incorporate speckle contour detection principles.*

For example, in the framework of Bayesian learning, introduction of *a priori* knowledge in the design of adaptive speckle filters has become a domain of growing interest, giving rise to a new class of Maximum *A Posteriori* (MAP) adaptive speckle filters [5], [11], [14], [15]. Among these filters, the well-known Refined Gamma-Gamma (to indicate Gamma pdfs for both speckle and noise-free reflectivity of the true scene) Maximum *A Posteriori* speckle filter (RGGMAP, [14], [15], [24]) improves the original GGMAP single-point filter expression by including structural detectors. These are (odd-symmetric) difference of boxes operators,

capable of detecting step edges, and even-symmetric operators, capable of detecting ridges, employed in the filtering process to delimit the homogeneous neighborhood on which local statistics are estimated [14]-[16]. An explicit dependence of adaptive speckle filters on speckle contour detectors is found in the class of adaptive speckle filters featuring region-based estimation of local statistics [24], [27]. These filters are two-stage procedures, the first stage performing segmentation and the second filtering. The first stage is a *hybrid segmentation module* consisting of: a) a contour detector incorporating a speckle model, such as the well-known Constant False Alarm (CFAR) edge detector [28]; and b) a (speckle model-free) segmentation module generating connected regions from non-connected contours based on geometric information exclusively (i.e., no radiometric values are employed at this stage) [6], [7], [24]. Next, the second stage of the filtering scheme applies a single-point adaptive speckle filter (e.g., GGMAP) whose local statistics are extracted from neighboring pixels belonging to the same segment as the pixel of interest.

4 State of the art in SAR image segmentation schemes

SAR image segmentation systems found in the literature can be divided into two main categories. *The first category employs a speckle filtering stage to generate a noise-free image, followed by a speckle model-free segmentation stage* [9], [19], [20]. Among these algorithms, the histogram-based segmentation method proposed in [19] as an improvement of the algorithm presented in [20] is interesting because it is simple and fully automatic. It is based on the iterative application of a feature-preserving speckle filter. The procedure is stopped when a multimodal histogram suitable for thresholding is obtained. This segmentation algorithm employs: i) an enhanced feature-preserving sigma filter [20], [22]; ii) an automatic procedure for detecting speckle standard deviation (sigma) from processed data; iii) a convergence criterion to stop the iterative filtering scheme; and iv) an automatic procedure for detecting histogram peaks as a function of speckle standard deviation. The first limitation of this procedure is that it relies heavily on the feature-preserving properties of its speckle filter. The second limitation is that it is incapable of detecting classes whose grey levels fall within a two-sigma range of the larger (more frequent) classes in the histogram (equivalent to histogram local maxima). This is tantamount to saying that this histogram-based method guarantees acceptable performances iff the image of interest depicts few well-separated (uniformly distributed) surface classes in the radiance domain.

The second category of SAR image segmentation systems found in the literature employs a SAR contour detector incorporating a speckle model without any prior filtering, followed by a speckle model-free segmentation stage [6], [7]. The CFAR edge detector, proposed in [28], is a well-known example of speckle model-based contour detector employed for segmentation purposes [6], [7], [24].

Since speckle contour detection principles are included in adaptive speckle filters (see Section 3), we consider the first class of SAR image segmentation algorithms, where an adaptive speckle filter is employed, as a subset of the second class of SAR image segmentation algorithms centered on speckle contour detection. As a consequence, *the rest of this paper is focused on the analysis of SAR image segmentation systems exploiting a contour detector as their first stage.* Additional observations may support this decision. With regard to computation time, edge detection methods are intrinsically parallel processes.

Moreover, design of local filters for edge detection features a strong theoretical foundation in signal processing theory and statistical analysis [29]-[32]. Finally, neurophysiology may provide useful information on how the mammalian Primary Visual Cortex (PVC) employs multi-scale filter banks in low-level vision [33]-[43]. This scenario is consistent with the multidisciplinary effort urged to develop the new science of complex systems [44].

It is to be observed that several segmentation algorithms presented in the literature to provide solutions that are statistically sound according to Bayes' rule do not satisfy the requirements of our SAR image segmentation task. In these algorithms a MAP estimate of a labeling solution, given the (noise-affected) observables, employs a Markov Random Field (MRF) model to capture known stochastic components of the labeled scene [12], [45], [46]. A MRF model by itself is not very useful, unless we provide a good model for class-conditional density (representing the degree to which the model of a class fits the data) [46]. For example, the class-conditional likelihood can be modeled as either a uniform or a slowly varying intensity affected by additive Gaussian noise [45], [46]. In these two cases parameters required to be known or estimated prior to segmentation are: the number of surface categories, their uniform intensity value (to be locally adapted during processing in [46]) and the standard deviation of additive Gaussian noise. Thus, these algorithms satisfy neither the multiplicative speckle model hypothesis nor our unsupervised learning requirements (see Section 1). Another class of MRF segmentation algorithms employs a textured region model for class-conditional likelihood. Since this approach is applicable only to noise-free textured images formed by known textures [45], it does not satisfy our unsupervised learning requirements either.

4.1 Assessment of the CFAR-based segmentation scheme

The hybrid segmentation procedure employed in [6] and [7] for classification purposes and in [24] for filtering purposes is fully automatic and based on the well-known, speckle model-based CFAR edge detector [28] (see Section 3). According to these observations the CFAR-based hybrid segmentation scheme is selected as a significant example in the class of SAR image segmentation systems based on contour detection. The selected segmentation scheme is tested on three coherent images acquired by different SAR sensors and featuring different contents of the scene. To assess how well the segmentation procedure fits the final goal of our treatment, i.e., segmentation for classification, we can only inspect the segmented output image qualitatively (see Section 7.1 for more details). On the other hand, in line with [24], the region-based GGMAP speckle filtering stage is applied in cascade to the segmentation block to assess how well the same CFAR-based segmentation scheme performs in a processing framework different from classification such as speckle filtering.

The scheme of CFAR is shown in Appendix 1 while its basic principles are summarized below [28]:

• In line with [18], the pdf of the speckled observed intensity for a homogeneous natural extended target is assumed to be equal to a Gamma distribution (rather than a K-distribution, see Section 2).

• A battery of (odd-symmetric) difference of boxes operators featuring increasing size windows (3×3, 5×5, 7×7, 9×9) and four different orientations (0, 45, 90 and 135^o) are employed to compute the oriented image gradient. It is known that difference of boxes

operators are optimal step edge detectors [47]. This implies that CFAR is not designed to optimally detect other image structures such as roofs and ramp edges [24], [40], [42].
• The activation function of each (difference of boxes) operator is defined as the minimum ratio between the two absolute values computed by convolving the image with the two opposite sides of the odd-symmetric filter. Thus, each activation value is a ratio (similarity) measure computed as a relative number, i.e., belonging to range (0,1): when the similarity measure is equal to one, then contrast (gradient) detected across the filter axis is zero, and vice versa.
• At a given resolution level, each oriented filter, centered on the pixel of interest, provides a ratio (similarity) measure to be compared with a scale-dependent theoretical ratio threshold based on the assumption that the speckled signal is homogeneous on the two opposite sides of the filter receptive field. If the filter activation value is below the theoretical ratio threshold (i.e., if the detected contrast is above a theoretical contrast threshold), then the central pixel is considered as belonging to an edge.

4.1.1 ERS-1 image

A spaceborn 3-look ERS-1 Precision Image (PRI), C-band, VV polarized, 512×512 pixels in size, with a pixel size of 12.5×12.5 meters, acquired November 14, 1992 (© ESA 1992), showing ice floes in the Bellingshausen Sea (Antarctica), is depicted in Fig. 1. The ENL value, providing a quantitative evaluation of the degree of speckle smoothing, was extracted from the image in Fig. 1 by exploiting the average of the ten smallest coefficient of variation values computed from local areas 9×9 pixels in size [22]. This automatic estimate provided an ENL value equal to 2.9. Fig. 2 shows contour pixels detected according to [28]. Fig. 3 shows the perimeters of the connected segments extracted from Fig. 2. Fig. 3, featuring $139 \cdot 374$ segments (where each contour pixel found in Fig. 2 is considered as a segment on its own), is clearly oversegmented for classification purposes. Fig. 4, featuring $ENL = 73$, shows the result of the region-based GGMAP speckle filtering. The filtered image is satisfactory both in terms of speckle noise removal and qualitative preservation of small structures. In other words, segmentation shown in Fig. 2 seems adequate when the final goal is speckle filtering, despite its inadequacy for classification purposes.

4.1.2 E-SAR image

An airborne 8-look E-SAR (Experimental SAR) image featuring 490×724 pixels in size and spatial resolution of 4.5×4.5 meters (Courtesy DLR-Germany) is shown in Fig. 5, where urban, agricultural and forest areas located around the airport of Oberpfaffenhofen, Germany, can be detected by the photointerpreter. Note that city areas are depicted as ordered textures, i.e., they consist of texels that can be either uniform or non-uniform in terms of size, orientation and density [48]. On the other hand, woodlands are depicted as disordered textures, i.e., they feature no texel, and should be investigated by a statistical model since they lack structure [48]. The ENL value extracted from this image is 16.7. Fig. 6 shows contour pixels detected according to [28]. Note that in both ordered and disordered textures (city areas and woodlands respectively) many contours are detected. Moreover, in line with theoretical failure modes of the algorithm (see Section 4.1), ramp edges and step edges featuring low contrast, e.g., between agricultural fields, are not detected in many

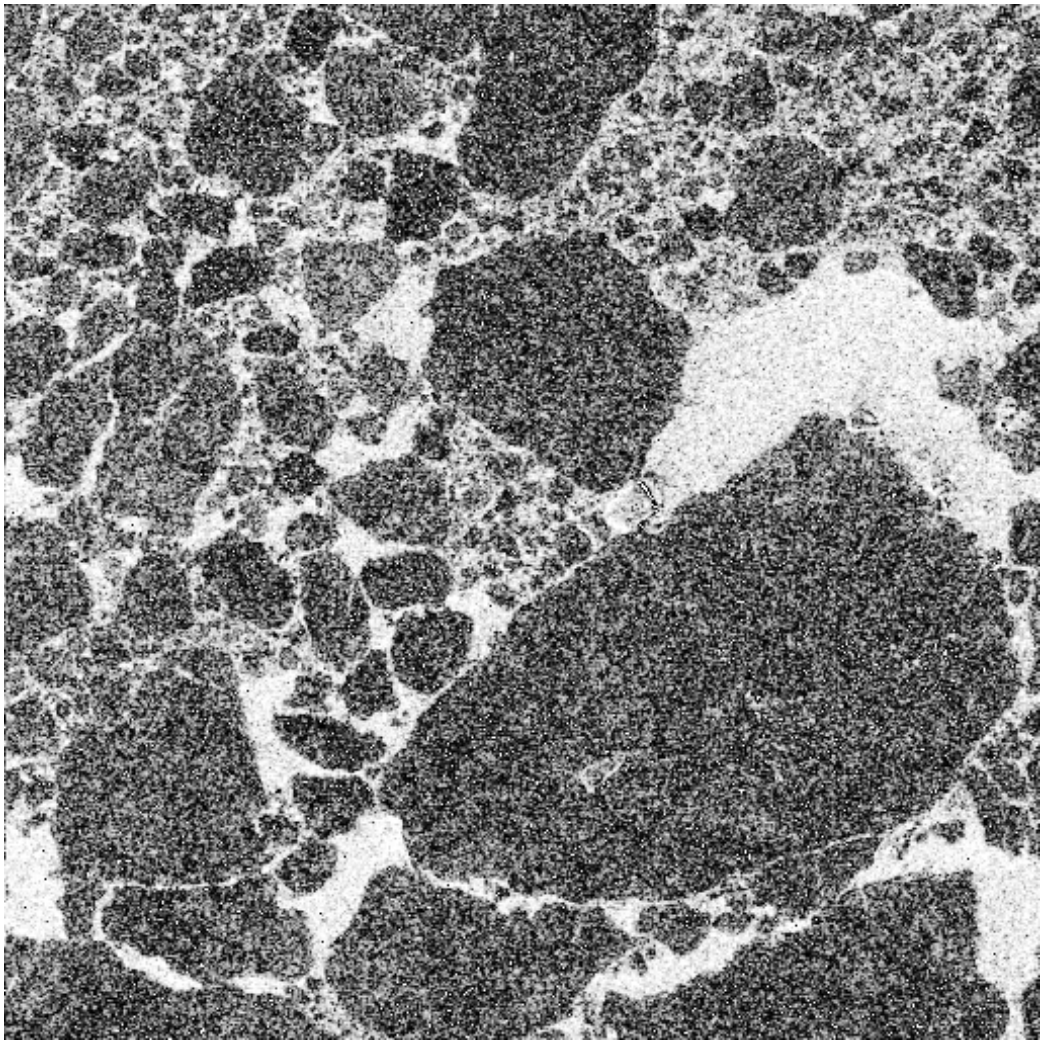

Figure 1: 3-look ERS-1 SAR image of the Bellingshausen Sea (Antarctica).

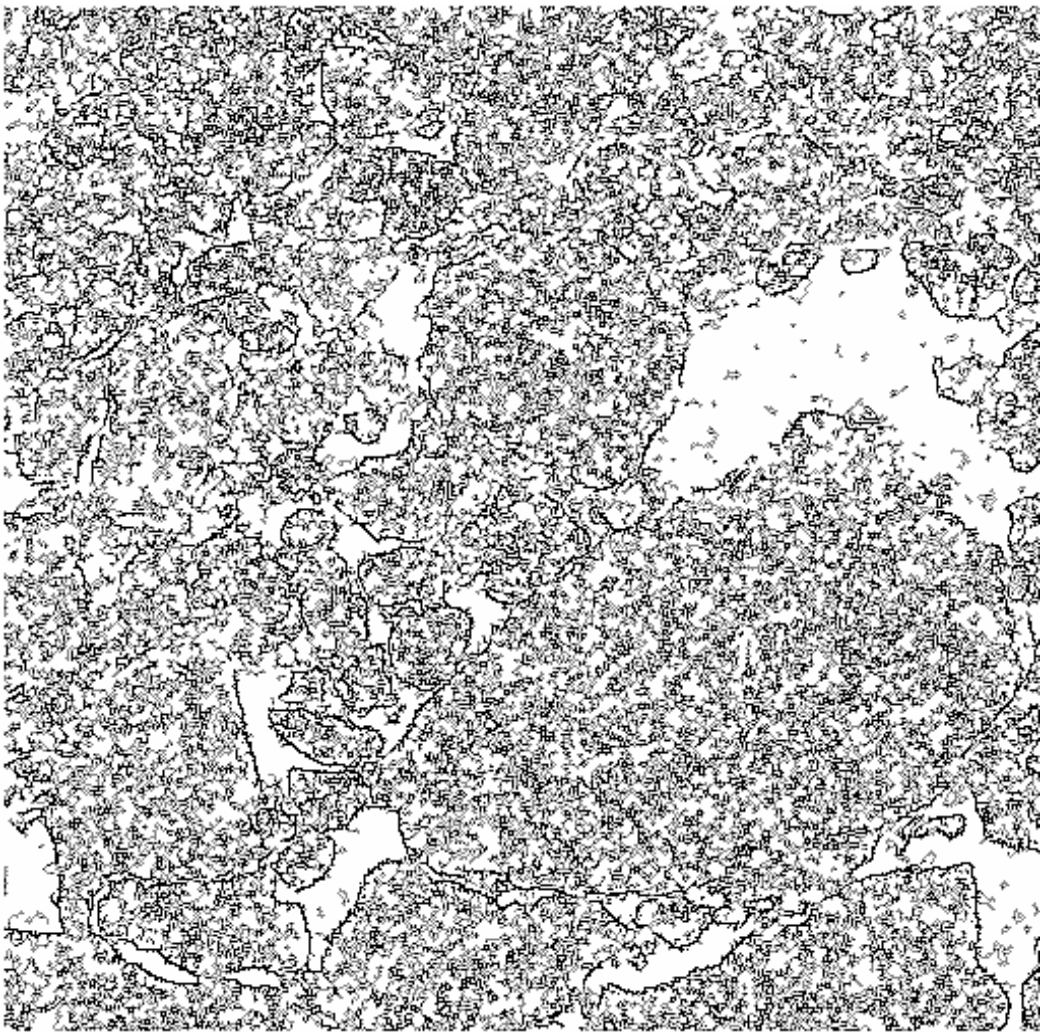

Figure 2: Contours of structural features detected by the speckle-based edge detectors.

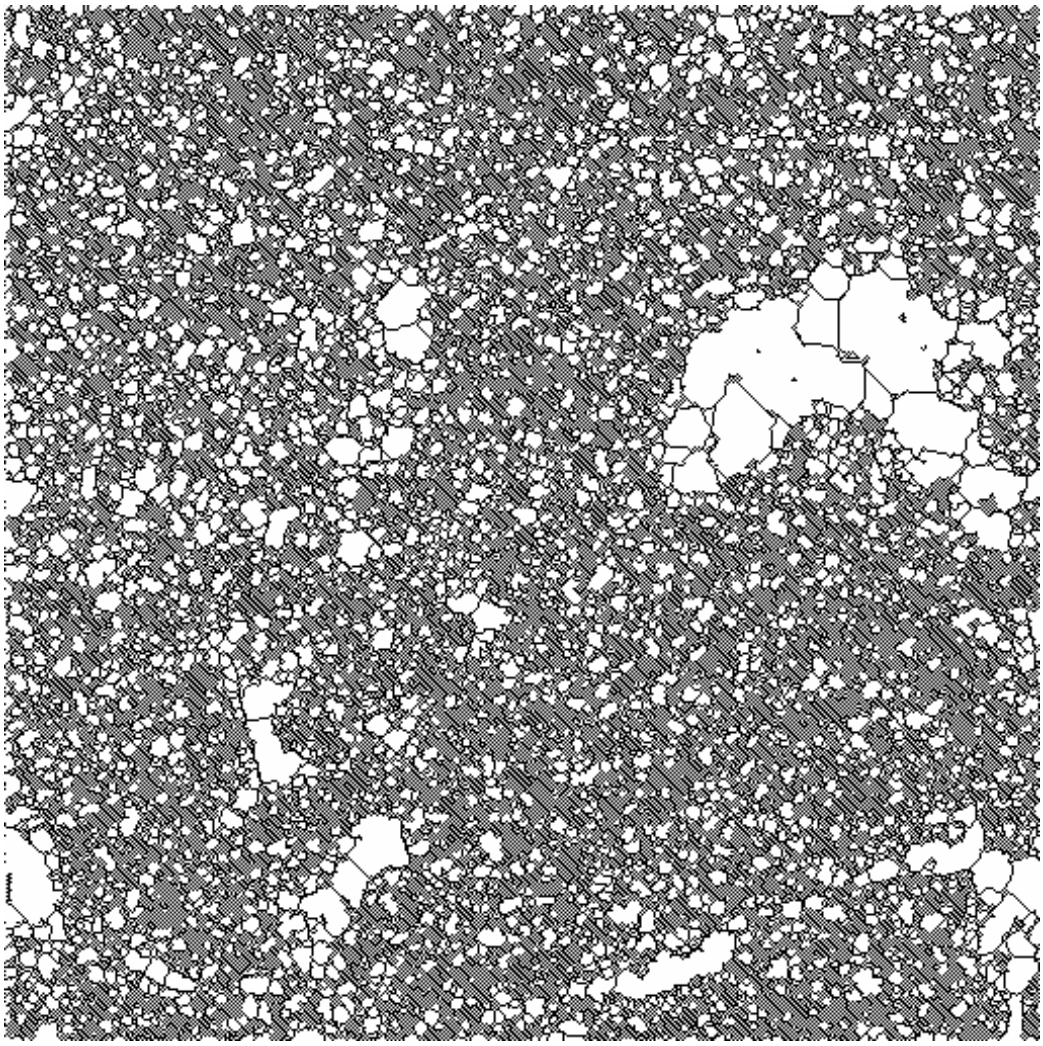

Figure 3: Segment boundaries extracted from non-connected contours shown in Fig. 2.

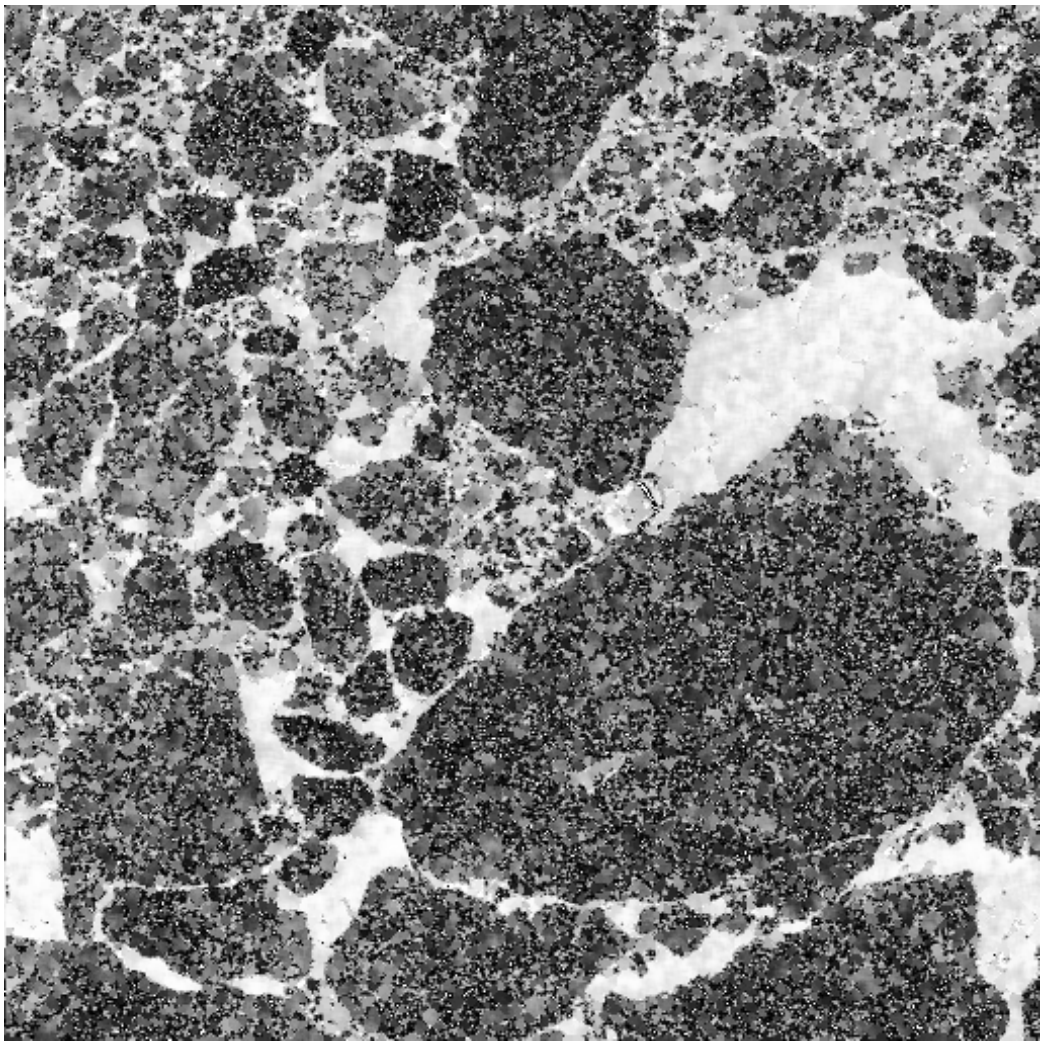

Figure 4: Region-based GGMAP speckle filter exploiting segments shown in Fig. 3.

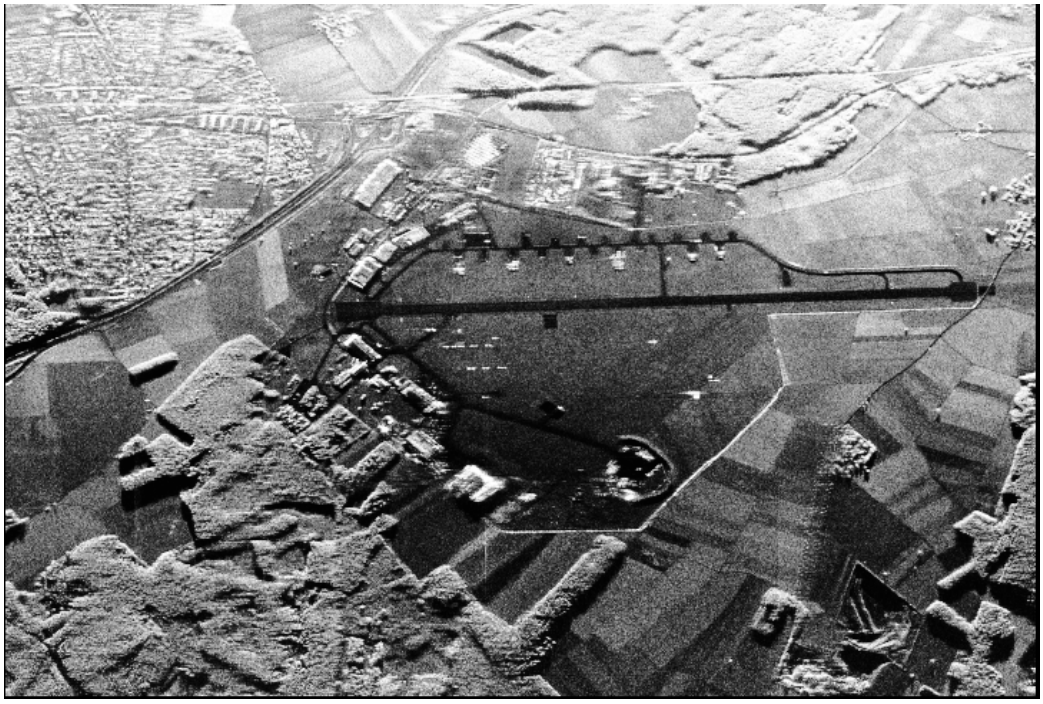

Figure 5: 8-look E-SAR image of the Oberpfaffenhofen area (Germany).

cases. Note that thin linear structures are properly detected instead. Fig. 7 shows the perimeters of the connected segments extracted from Fig. 6. Fig. 7, featuring 142·055 segments (where each contour pixel found in Fig. 6 is considered as a segment on its own), is clearly oversegmented for classification purposes. Fig. 8, featuring $ENL = 800$, shows the result of region-based GGMAP speckle filtering [24]. The filtered image is satisfactory both in terms of speckle noise removal and qualitative preservation of small structures. We conclude that, in line with the previous example where a spaceborne SAR image was processed, in this airborne SAR image example the segmentation process is considered inadequate for classification purposes, although it is effective in the framework of speckle filtering.

4.1.3 C-SAR image

An airborne 6 meter spatial resolution, 7-look, C-SAR (© Canada Center for Remote Sensing 1987) image of the area around Thetford (UK), acquired during the Agriscatt 87 Experiment campaign, 400×400 pixels in size is shown in Fig. 9. Urban, agricultural and forest areas can be recognized. The ENL value extracted from this image is 6.6. Fig. 10 shows contour pixels detected according to [28]. Note that in both ordered and disordered textures (city areas and woodlands respectively) many contours are detected. Moreover, in line with the previous airborne image example, ramp edges and step edges featuring low contrast, e.g., between agricultural fields, are not detected in many cases. Detection of thin linear structures seems satisfactory. Fig. 11 shows the perimeters of the connected segments extracted from Fig. 10. Fig. 11, featuring 60·786 segments (where each contour

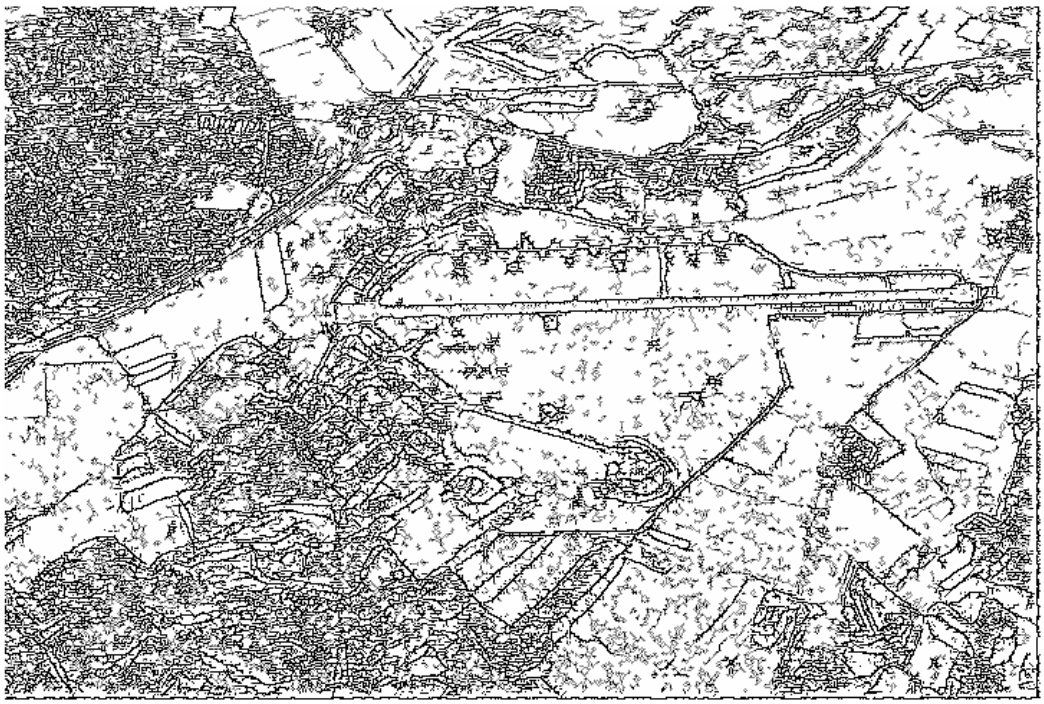

Figure 6: Contours of structural features detected by the speckle-based edge detectors.

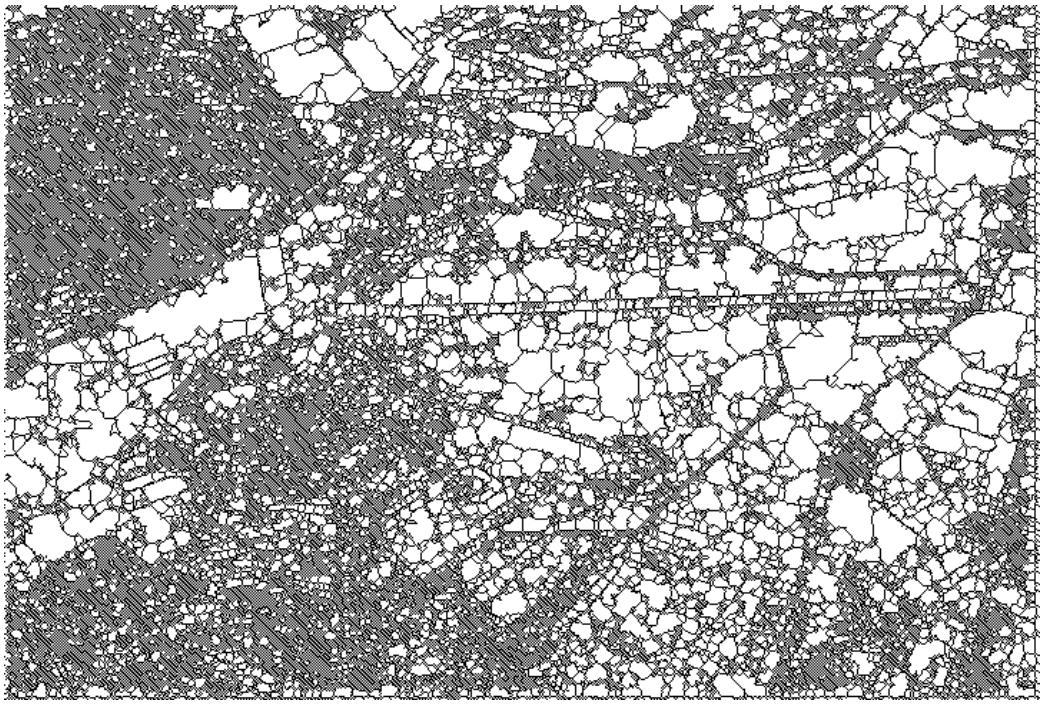

Figure 7: Segment boundaries extracted from non-connected contours shown in Fig. 6.

Figure 8: Region-based GGMAP speckle filter exploiting segments shown in Fig. 7.

pixel found in Fig. 10 is considered as a segment on its own), is clearly oversegmented for classification purposes. Fig. 12, featuring $ENL = 370$, shows the result of region-based GGMAP speckle filtering [24]. The filtered image is satisfactory both in terms of speckle noise removal and qualitative preservation of small structures. In line with the two previous examples, segmentation considered inadequate for classification purposes proved to be effective in speckle filtering.

5 Modifying the SAR image segmentation scheme

The hybrid segmentation algorithm employed in Section 4 shows that CFAR is sensitive to edges that can be considered false edges in a classification framework. Moreover, CFAR employs a complex hierarchy of edge thresholding decisions (see Appendix 1); therefore, it is unreasonable to provide the end user with a non-automatic version of CFAR whose (four) thresholds are user-defined interactively. Our idea is to provide the hybrid segmentation scheme employed in Section 4 with a contour detector selected from the literature that satisfies the following constraints: i) it is less affected than CFAR by false edges within the framework of a segment-based SAR image classification task; and ii) its thresholding strategy makes it easy to use.

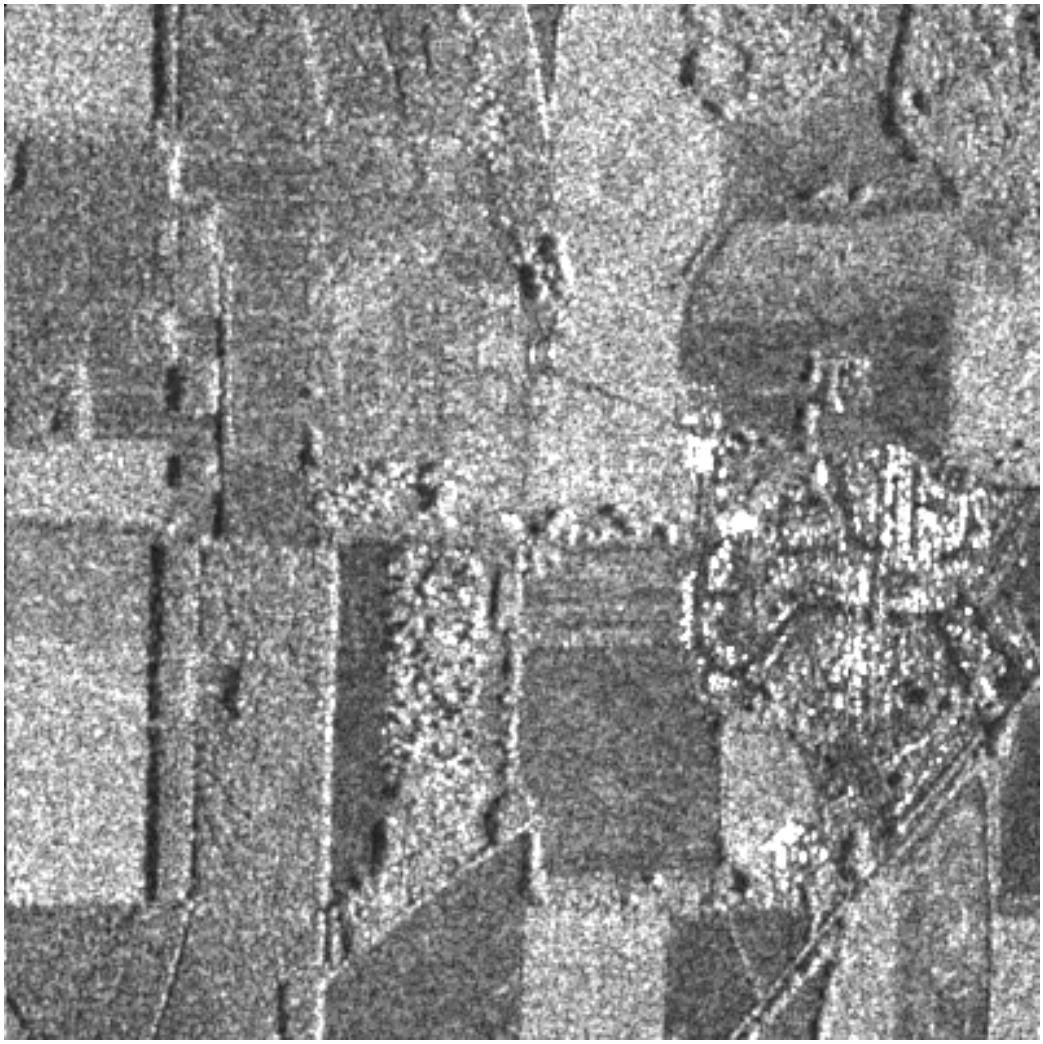

Figure 9: 7-look C-SAR image of the Thetford area (UK).

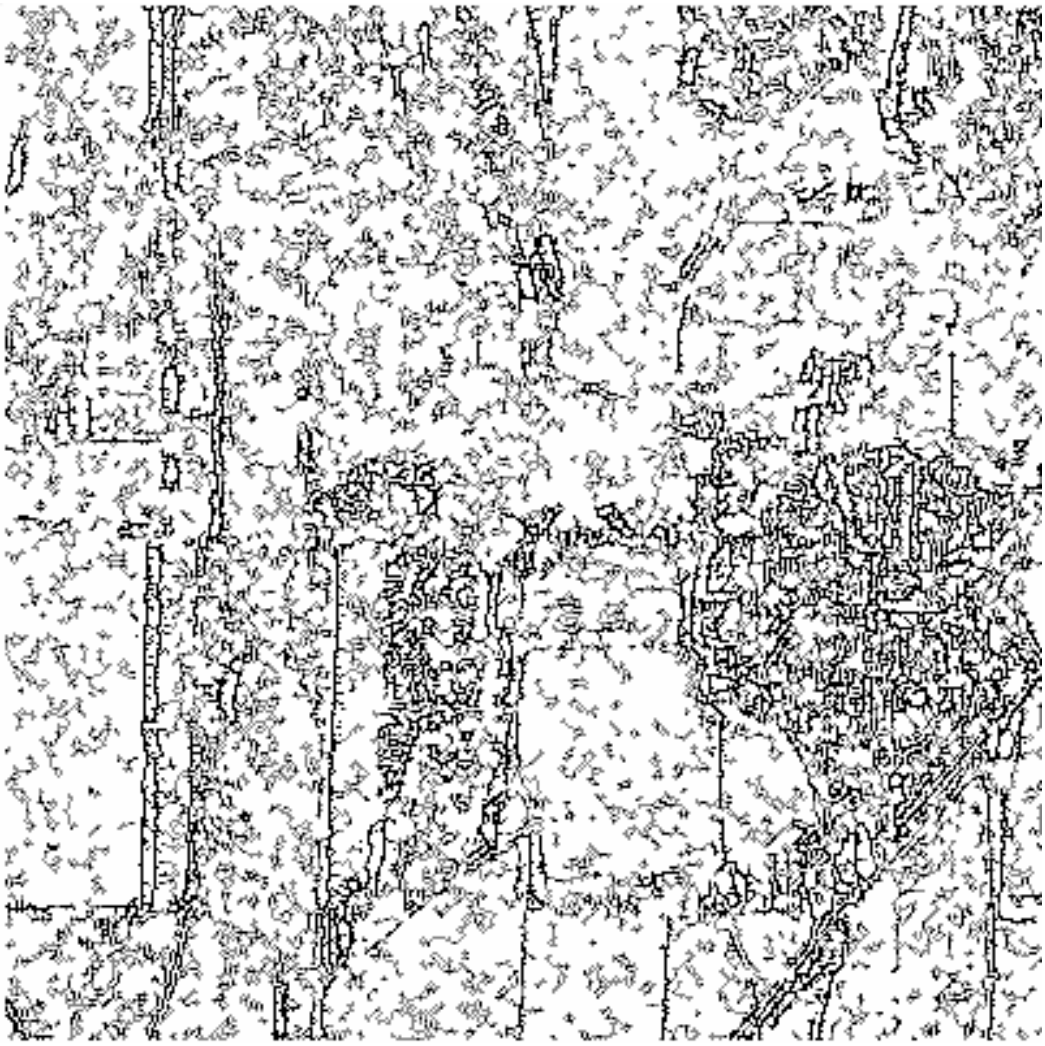

Figure 10: Contours of structural features detected by the speckle-based edge detectors.

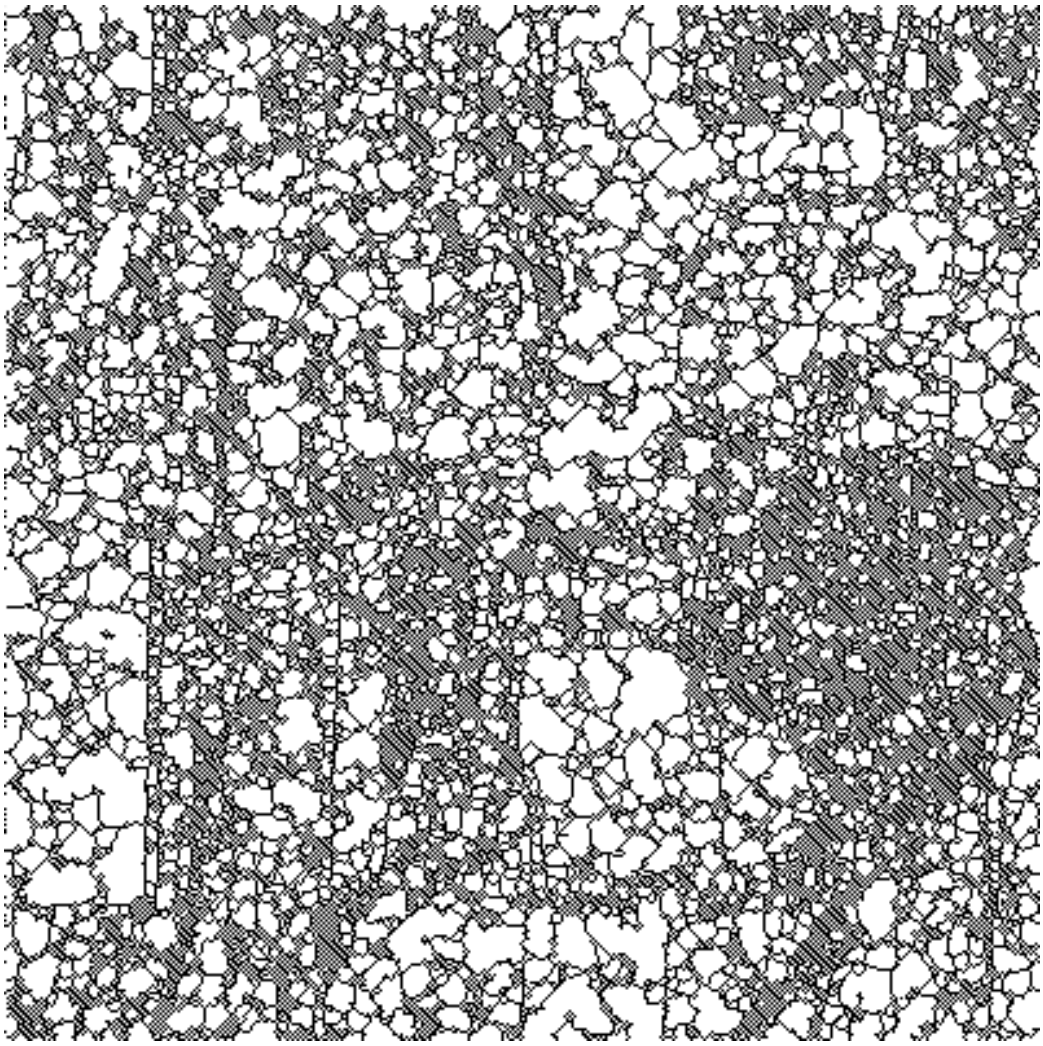

Figure 11: Segment boundaries extracted from non-connected contours shown in Fig. 10.

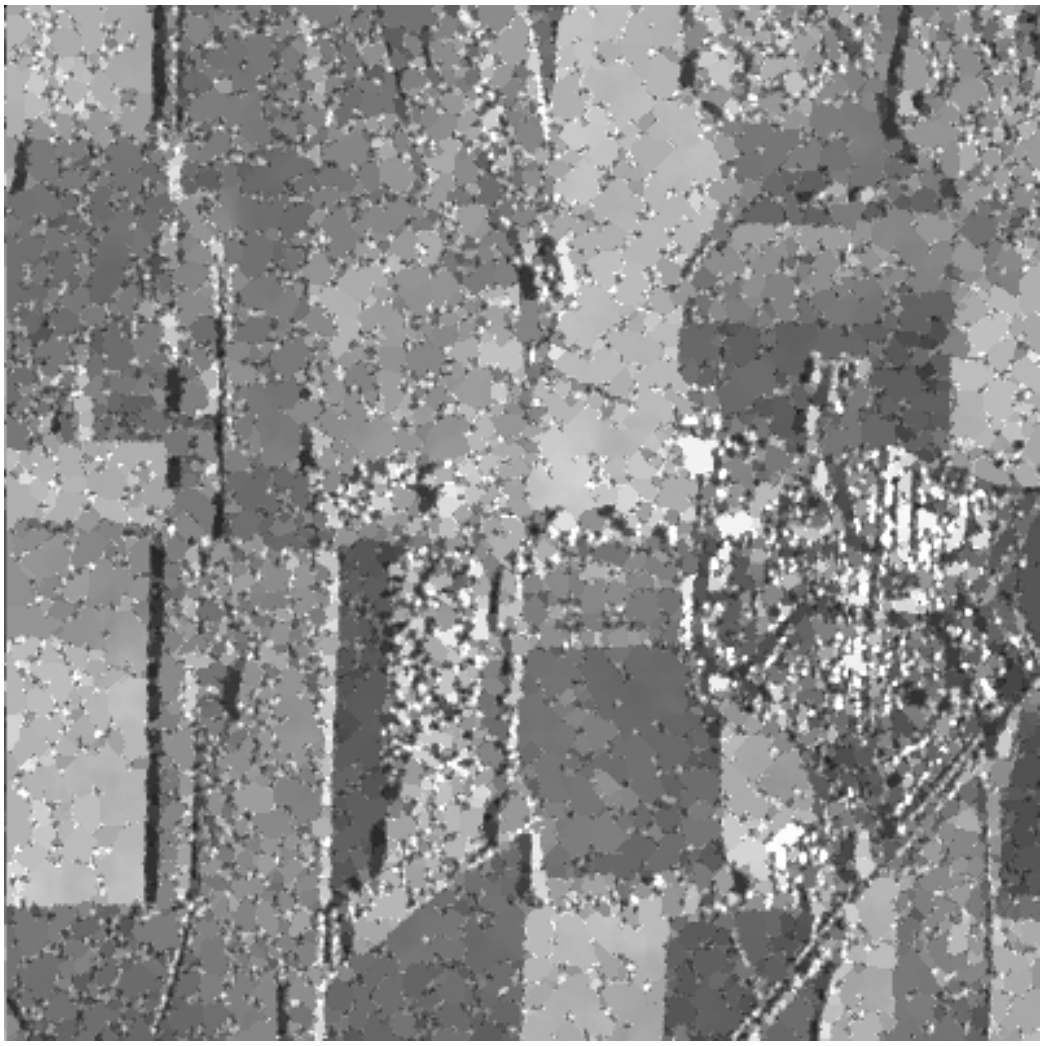

Figure 12: Region-based GGMAP speckle filter exploiting segments shown in Fig. 11.

5.1 A review of contour detectors

Some basic concepts involved with edge detection methods found in the literature are briefly reviewed. In [47], odd-symmetric edge detectors and even-symmetric ridge detectors were developed to optimize signal-to-noise ratio and localization criteria. The difference of boxes operator, which is incidentally employed in RGGMAP and CFAR (see Sections 3 and 4.1 respectively), was considered to be optimal for detecting step edges. However, due to its very large bandwidth, this operator features very marked effects for large operator sizes; therefore, substitution of this operator with an odd-symmetric filter featuring limited bandwidth (e.g., first derivative of a Gaussian) is recommended [47]. In [47] no effective solution for combining detection properties of step edge and ridge operators was found. In computer vision literature, contour and texture detectors employ even- and odd-symmetric filters either computed as quadrature pairs [29], [30], [40], [49], or as complex Gabor functions [42], [48], [50], [51]. It is known that Gabor functions provide band-pass filters working in a joint space/spatial-frequency domain (such that a Gaussian frequency window band-passes the spatial-frequency content of an image area localized by a Gaussian data window sliding across the 2-D spatial domain). An important development has been proposed in [40] and [49], where the two outputs of an even- and odd-symmetric filter pair are combined by a nonlinear Phytagorean sum to compute local energy, which has proved to be an optimal measure with respect to a variety of edge types (step edges, ridges, ramps, roofs). This combination has led to the development of *image processing algorithms combining responses of even- and odd-symmetric filter pairs to detect contours of structural elements (step edges, ridges, ramps, roofs) at high resolution scales* [29], [30], [40], *and texture transitions at lower spatial resolutions* [48], [50], [51]. In [42], the contour detector is capable of processing both monochromatic and multi-spectral images and is, therefore, termed Chromatic and Achromatic Contour Detector (CACD). For each pixel of interest CACD applies a battery of oriented operators working at two spatial scales (separated by one octave in the frequency domain; possible filter sizes are, in pixel units, 3, 7, 13, 25 etc.). Operators are odd- and even-symmetric filter pairs defined, respectively, as the imaginary and real part of a "zero dc component" complex Gabor function (i.e., featuring zero output to constant input). Every odd- and even-symmetric filter computes an activation value belonging to range (0,1) and is proportional, respectively, to the oriented first (contrast) and second derivative (change of contrast) of image intensity (in case of multi-spectral images, this activation value is actually a combination of a chromatic color contrast term with an achromatic color contrast component). Next, activation values of each pair of odd- and even-symmetric filters are combined by a nonlinear Phytagorean sum to compute a local energy term as a real number in range (0,1). Finally, CACD employs a coupling mechanism among energy terms. In particular, it adopts a competitive mechanism among filter pairs featuring: i) different orientations, but the same size (cross-orientation inhibition, [49]); and ii) the same orientation, but different sizes. It is to be noted that CACD analyzes the continuous values of the second derivative of image intensity to perform consistently with the psychophysical phenomenon of Mach bands[1] in detecting ramps and roofs [40]. This result is not obvious insofar as in the literature many contour detection algorithms simply detect those points

[1] Where a luminance (radiance, intensity) ramp meets a plateau, there are spikes of brightness (perceived luminance), although there is no discontinuity in the luminance profile.

where the second derivative of image intensity is equal to zero (i.e., where the first derivative presents a local maximum) [31], [47].

The first conclusion emerging from this brief review of contour detectors is that *the combination of even- and odd-symmetric filters working at different scales of analysis, rather than their separate processing*, is fundamental in detecting image structures as well as texture boundaries [24]. The second observation is that speckle model-based CFAR employs a completely generic filter bank consisting of odd-symmetric (difference of boxes) filters to compute the oriented first derivative of image intensity. What is domain-specific in CFAR is its scale-dependent, hierarchical thresholding strategy, where *a priori* (background) knowledge on speckled radiance is introduced to compute theoretical similarity (contrast) thresholds below (above) which the presence of a step edge is detected by a difference of boxes operator.

5.2 Assessment of the CACD-based segmentation scheme

Owing to its interesting functional properties, we intend to verify whether CACD is less sensitive than CFAR to the presence of false edges in the framework of a segment-based SAR image classification task. The segmentation approach that exploits CACD as its first processing block is the same as that employed in Section 4 [6], [7], [24]. In our experiments the two resolution levels of the local filters employed by CACD are selected equal to 13 and 25 pixels respectively.

5.2.1 ERS-1 image

Fig. 13 shows the output contour image generated by CACD when Fig. 1 is processed and a user-defined Contrast Threshold, C_{TH}, is properly selected as a relative number in range (0,1) (in this example, $C_{TH} = 0.09$). Fig. 14 shows the perimeters of the connected segments extracted from Fig. 13. Fig. 14, featuring $20 \cdot 348$ segments (where each contour pixel found in Fig. 13 is considered as a segment on its own), is less fragmented than Fig. 3, but it is still affected by artifacts and is clearly oversegmented for classification purposes. Fig. 15, featuring $ENL = 195$, shows the result of region-based GGMAP speckle filtering [24]. When compared to Fig. 4, Fig. 15 shows that some thin/small image details are removed or blurred; thus, a refinement in the strategy employed by CACD to combine multi-scale filter signals is recommended. This new strategy should also improve CACD performance in detecting T- and X-junctions. Nonetheless, Fig. 14 appears to be more feasible than Fig. 3 for classification purposes. In terms of computation time, the use of CACD in place of CFAR allows a significant reduction ($\approx 85\%$) in the number of segments to be further reduced by time-consuming region growing blocks employed in cascade.

5.2.2 E-SAR image

Fig. 16 shows the output contour image generated by CACD when Fig. 5 is processed and C_{TH} is set to 0.02. Owing to its combination of odd- and even-symmetric filter pair signals, CACD is effective in detecting ramp edges and low contrast step edges between agricultural fields. On the other hand, thin linear structures are not extracted properly. The attempt at running a CACD version employing filter sizes equal to 3 and 6 pixel units

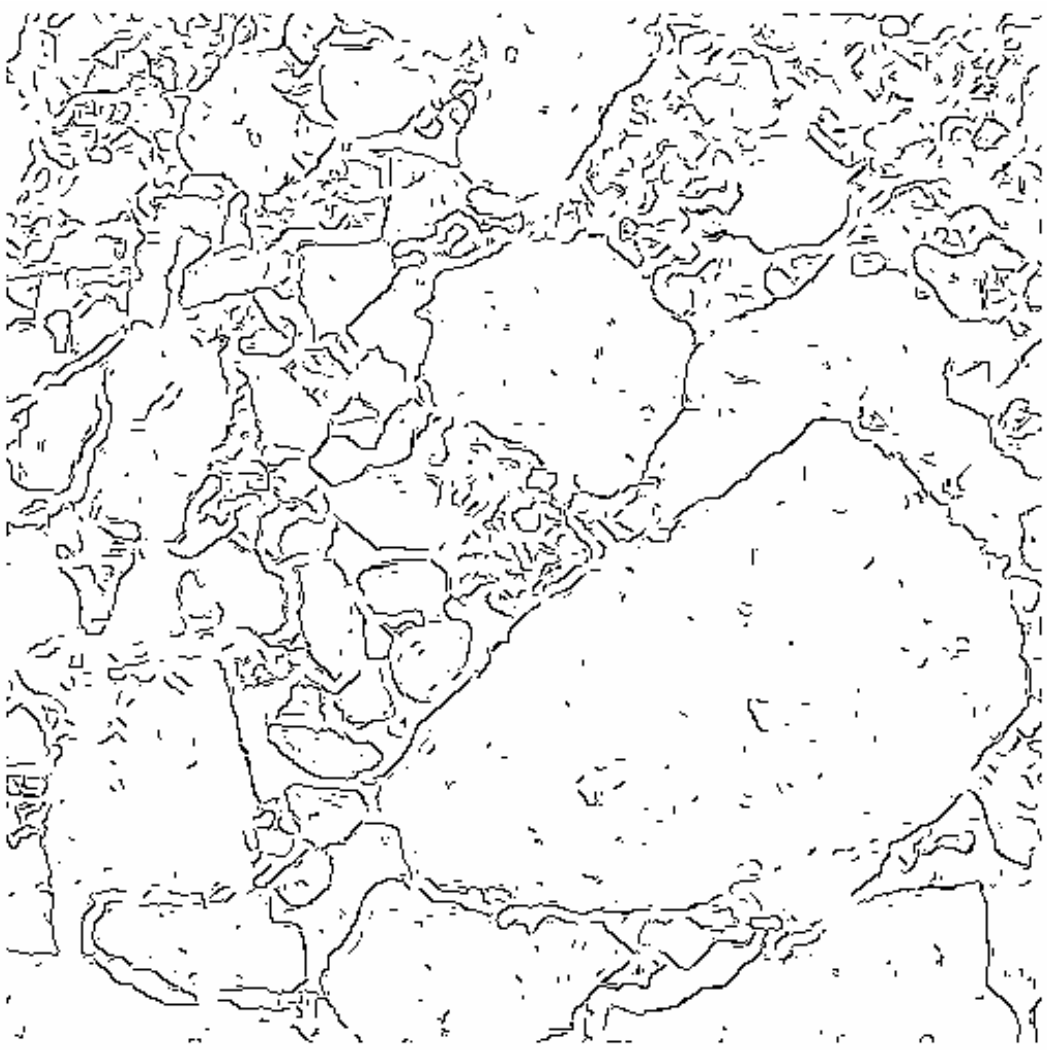

Figure 13: Contours of structural features detected by CACD.

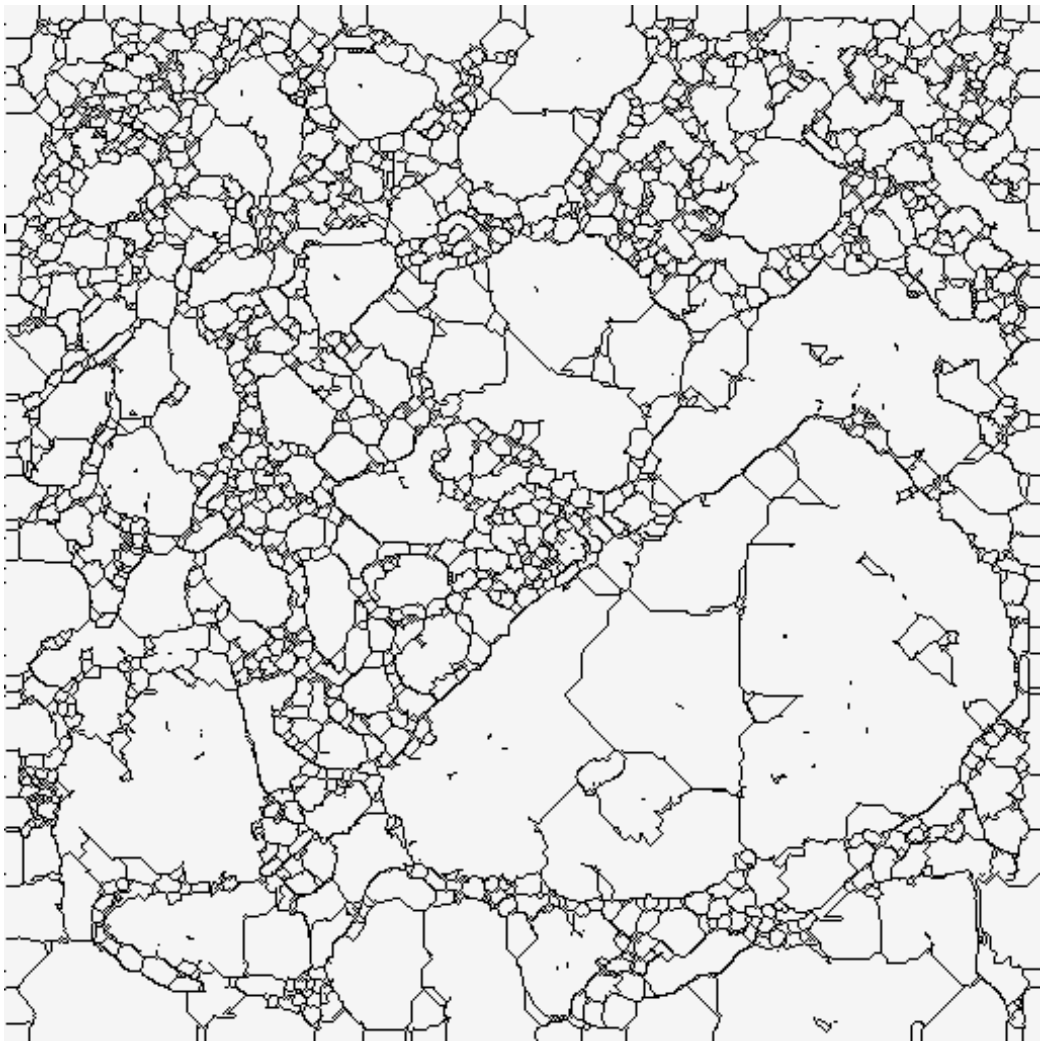

Figure 14: Segment boundaries extracted from non-connected contours shown in Fig. 13.

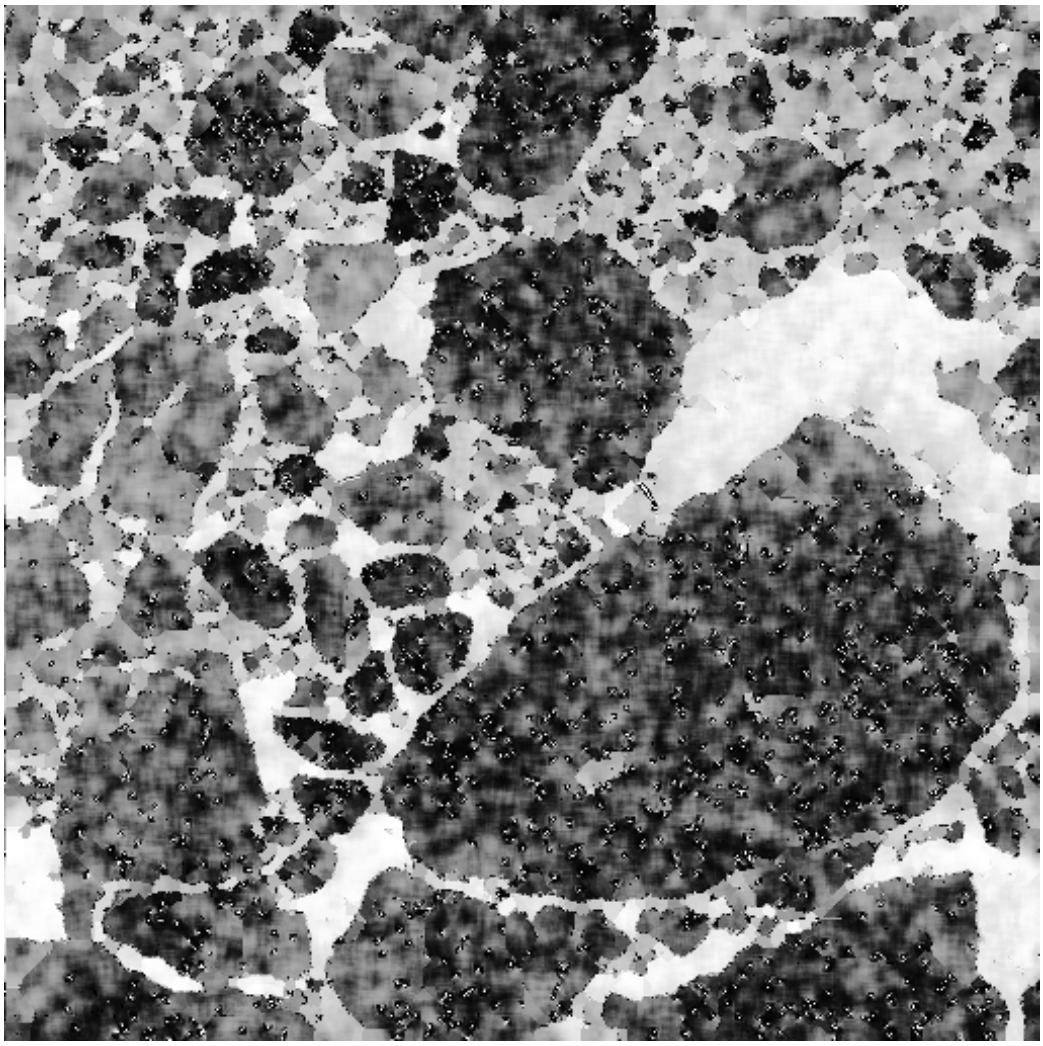

Figure 15: Region-based GGMAP speckle filter exploiting segments shown in Fig. 14.

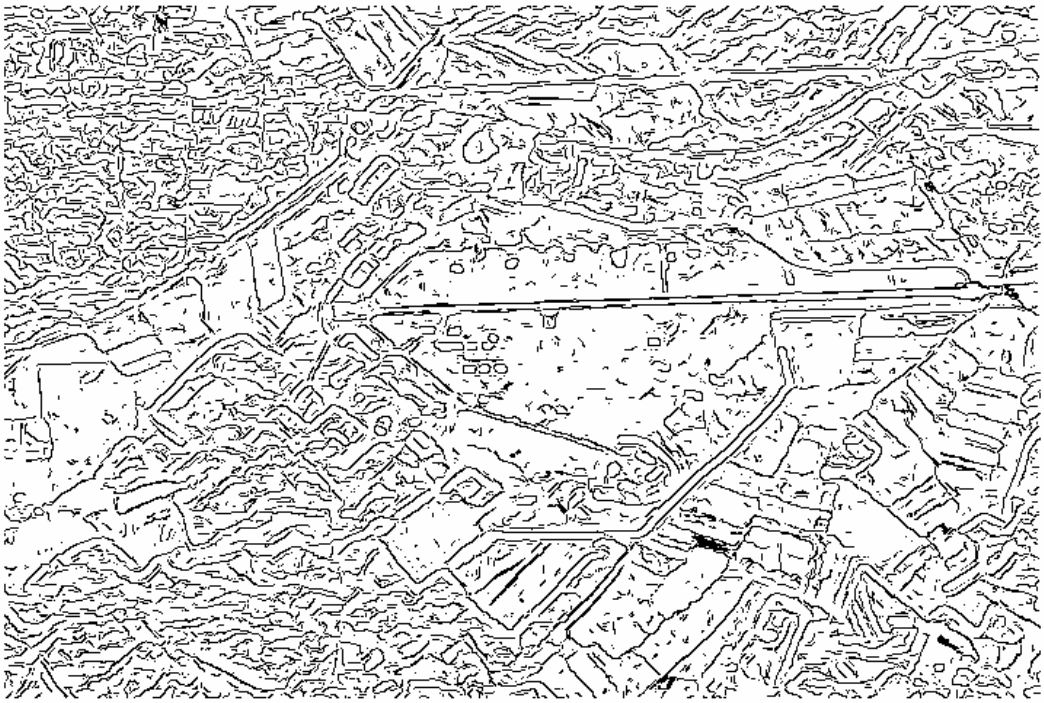

Figure 16: Contours of structural features detected by CACD (filter sizes: 13, 25).

would not solve this problem, as shown in Fig. 17, where C_{TH} is set to 0.02. Fig. 18 shows the perimeters of the connected segments extracted from Fig. 16. Fig. 18, featuring $63 \cdot 534$ segments (where each contour pixel found in Fig. 16 is considered as a segment on its own), is less fragmented than Fig. 7, but it is still affected by artifacts and clearly oversegmented for classification purposes. Fig. 19, featuring $ENL = 1240$, shows the result of region-based GGMAP speckle filtering [24], where some thin/small image details are removed or blurred. In line with the first spaceborne SAR image example, this airborne SAR image case confirms that the strategy employed by CACD to combine multi-scale filter signals must be improved. In terms of computation time, the use of CACD in place of CFAR allows a significant reduction ($\approx 55\%$) in the number of segments to be further reduced by time-consuming region growing blocks employed in cascade.

5.2.3 C-SAR image

Fig. 20 shows the output contour image generated by CACD when Fig. 9 is processed and C_{TH} is set to 0.06. Thin linear structures are not extracted properly. Fig. 21 shows the perimeters of the connected segments extracted from Fig. 20. Fig. 21, featuring $21 \cdot 844$ segments (where each contour pixel found in Fig. 20 is considered as a segment on its own), although less fragmented than Fig. 11, is still affected by artifacts and clearly oversegmented for classification purposes. Fig. 22, featuring $ENL = 1150$, shows the result of region-based GGMAP speckle filtering [24], where some thin/small image details are removed or blurred. In line with the previous test cases, this airborne SAR example confirms that the strategy employed by CACD in combining multi-scale filter signals must be improved. In terms of

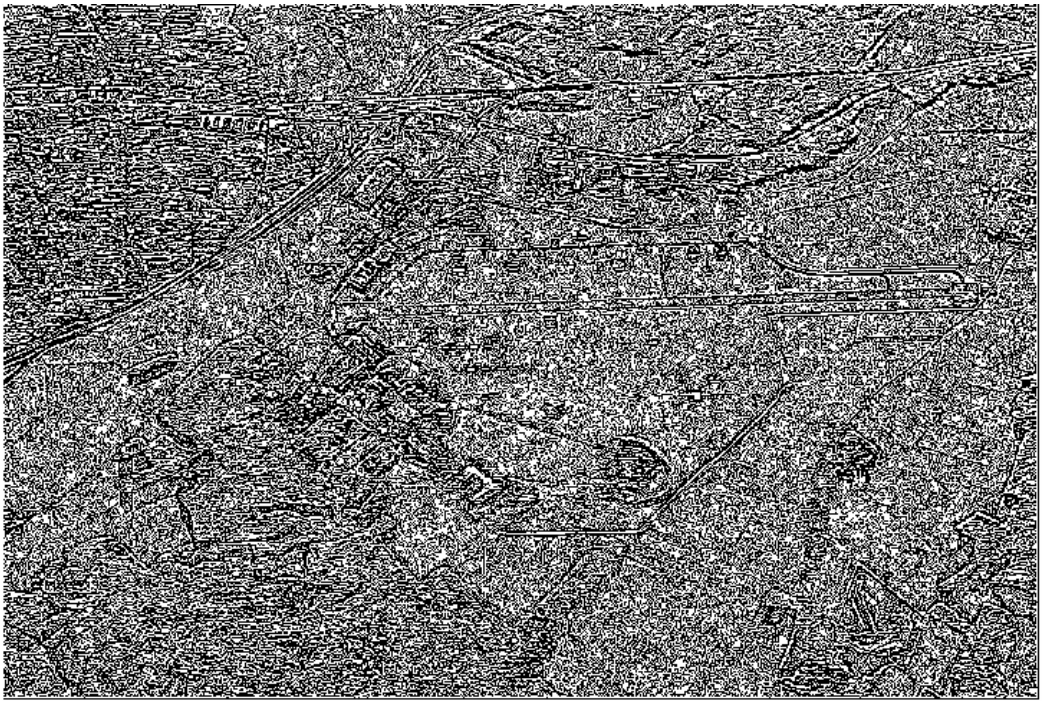

Figure 17: Contours of structural features detected by CACD (filter sizes: 3, 6).

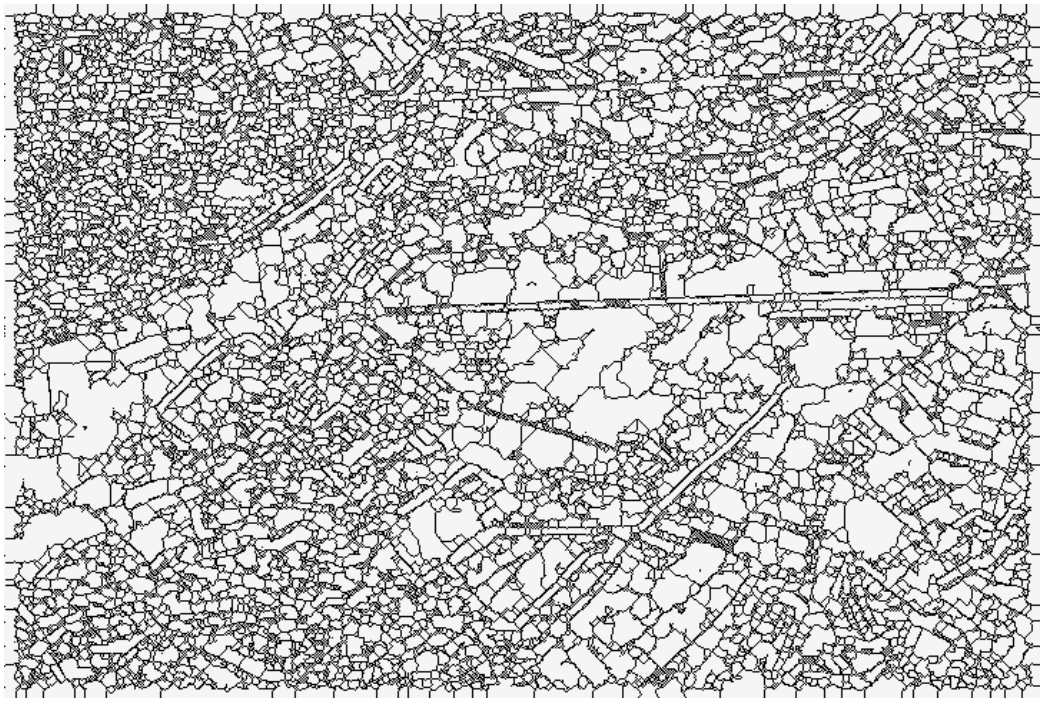

Figure 18: Segment boundaries extracted from non-connected contours shown in Fig. 16.

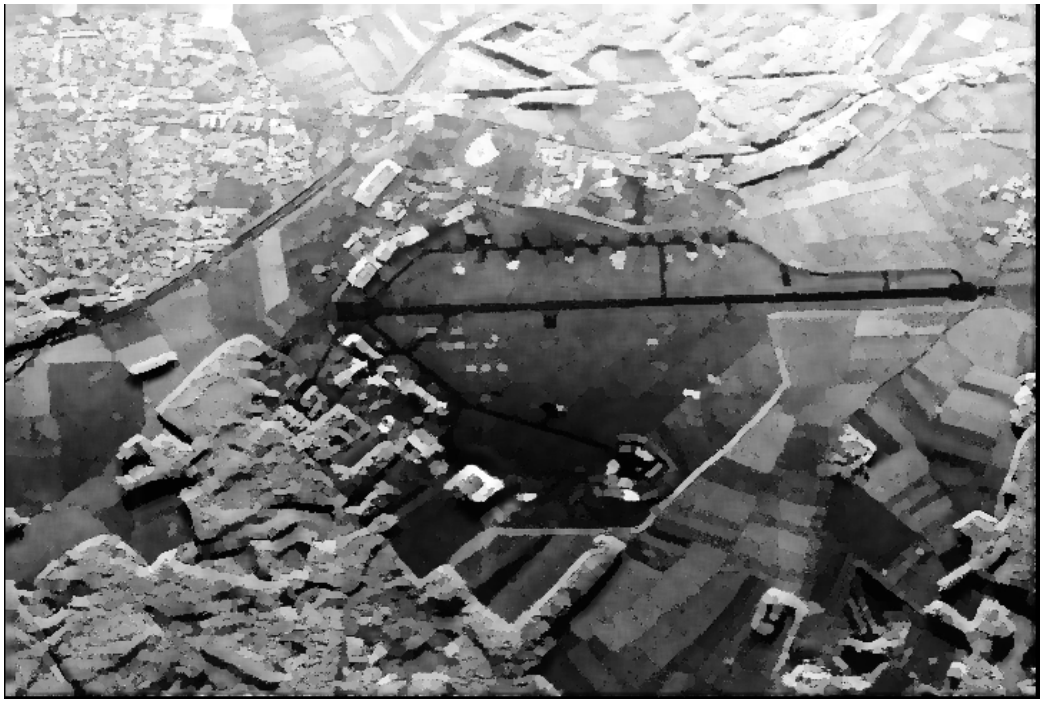

Figure 19: Region-based GGMAP speckle filter exploiting segments shown in Fig. 18.

computation time, the use of CACD in place of CFAR allows a significant reduction ($\approx 77\%$) in the number of segments to be further reduced by time-consuming region growing blocks employed in cascade.

6 Implementing a SAR image segmentation scheme

Within the hybrid segmentation scheme proposed in [6], [7], [24], CFAR exploits prior knowledge concerning speckle and is fully automatic, but it generates images that are over-segmented for classification purposes. Besides, a non-automatic version of CFAR is not conceivable, as it would require the end user to fine-tune a complex hierarchy of decisions regarding edge thresholding. On the other hand, CACD employs no prior information about the data source and is easy to use, requiring the user to select only one threshold as a relative number. In the framework of a SAR image classification task, substitution of CFAR with CACD has been seen to reduce oversegmentation phenomena, although small spatial details are lost, especially at airborne SAR resolution. Our proposal is to employ CACD as the core of a speckle model-free SAR image segmentation scheme that takes its inspiration from the SAR filtering procedure proposed in [24]. Since artifacts generated when segments are extracted from non-connected contours are not acceptable in a classification framework (while they are more acceptable when speckle filtering is the final goal of the treatment, see Figs. 4, 8, 12), region merging blocks capable of eliminating artifacts must be added to the basic segmentation scheme proposed in [6], [7], [24]. Incidentally, since CACD works on both monochromatic and multi-spectral optical images, we propose a unified framework capable

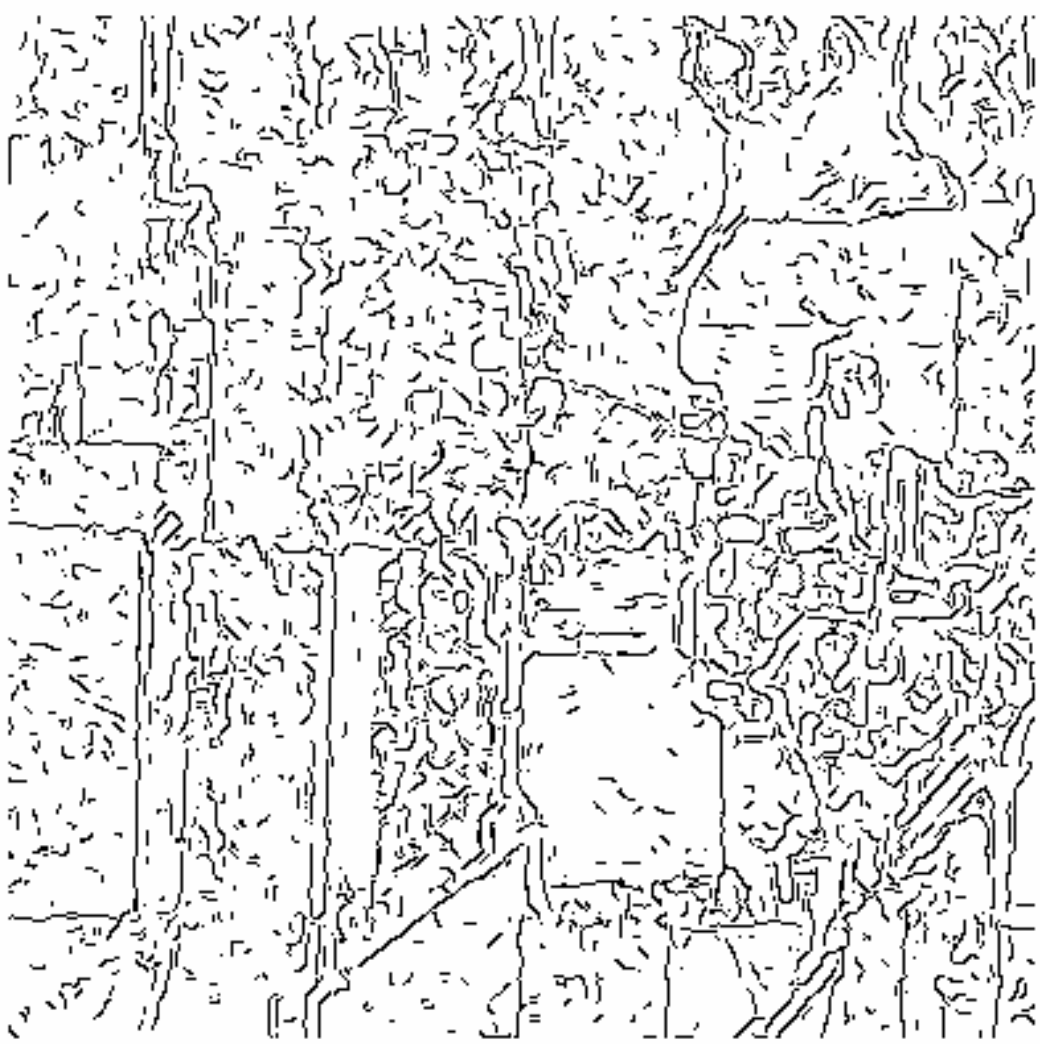

Figure 20: Contours of structural features detected by CACD.

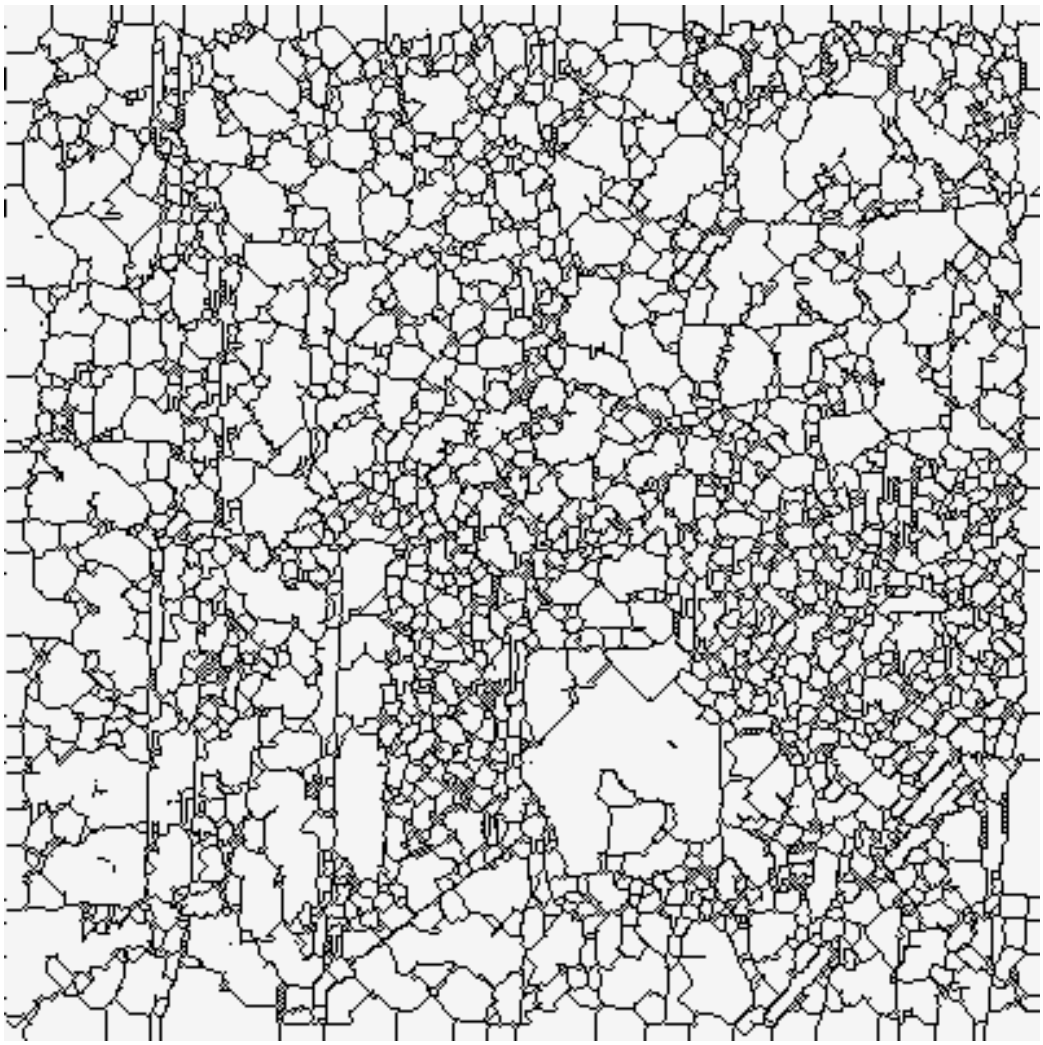

Figure 21: Segment boundaries extracted from non-connected contours shown in Fig. 20.

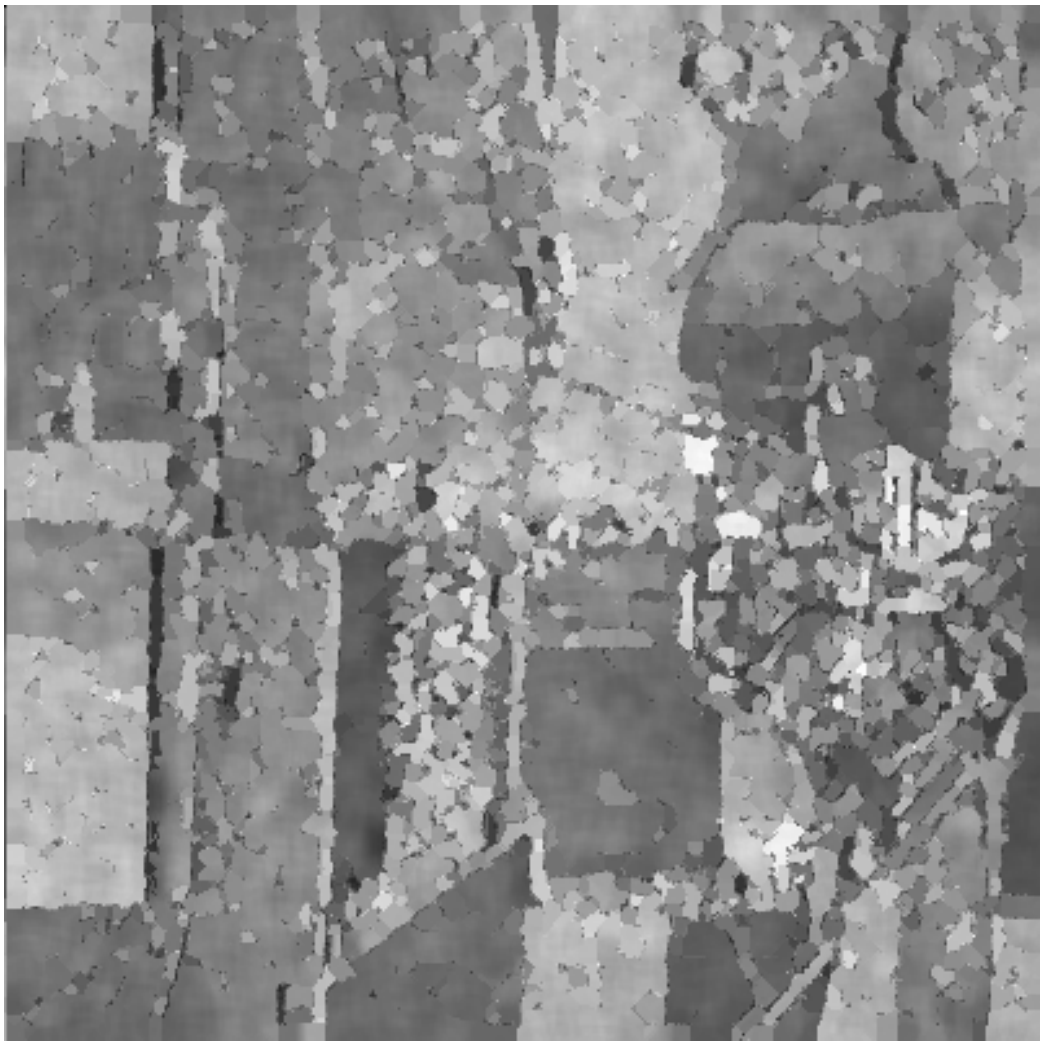

Figure 22: Region-based GGMAP speckle filter exploiting segments shown in Fig. 21.

of segmenting: i) incoherent (optical) or coherent (SAR) images; and ii) multi-spectral or monochromatic images.

To reduce oversegmentation, a variety of segment-merging approaches can be found in the literature [9], [52]-[56]. Basically, these methods are based on: i) heuristic segmentation criteria, i.e., they do not minimize any known objective function; and ii) merging constraints exploiting segment-based information such as: a) topology (e.g., adjacency between segments); b) shape; c) size; d) within-segment nth-order statistics, where n is not larger than 3, to try to capture segment-based textural properties [42], [57]-[59]; and e) segment boundary conditions [60].

We make up a region growing procedure by selecting two algorithms from the literature: i) the Low Contrast Segmentation (LCS) algorithm, exploiting *local statistics* to detect segments featuring smooth within-segment contrast [53], [54]; and ii) a self-organizing clustering neural network to detect *global image properties* as statistical regularities in within-segment statistics [58], [61], [62].

From the user point of view the interesting property of these two algorithms is that they both need one single parameter to run (actually, the neural network also requires a threshold on the maximum number of training epochs which can be set by the application developer). Both parameters consist of an inter-segment similarity threshold equivalent to a relative number belonging to range (0,1). For implementation details refer to the literature.

7 Segmentation results

The complete segmentation scheme proposed in Section 6 is tested on the three coherent images processed in Section 5.2. The robustness of the segmentation method is assessed by changing only one parameter of the procedure in the different experiments. This parameter is contrast threshold $C_{TH} \in (0, 1)$ required by CACD. This also implies that the similarity threshold employed by each of the two region growing stages (see Section 6) is fixed to a conservative value: in our experiments, this similarity threshold is set equal to 0.7 for both LCS and the clustering neural network.

Using the ERS-1 raw image shown in Fig. 1 and the segmented image shown in Fig. 14 as input, the proposed region growing procedure reduces the number of segments from $20{\cdot}348$ to $16{\cdot}811$ ($\approx 17\%$). The segmented output image is shown in Fig. 23, where most segment artifacts have been removed. Using the E-SAR raw image shown in Fig. 5 and the segmented image shown in Fig. 18 as input, the proposed region growing procedure reduces the number of segments from $63{\cdot}534$ to $35{\cdot}853$ ($\approx 43\%$). The segmented output image is shown in Fig. 24. Using the C-SAR raw image shown Fig. 9 and the segmented image shown in Fig. 21 as input, the proposed region growing procedure reduces the number of segments from $21{\cdot}844$ to $13{\cdot}860$ ($\approx 36\%$). The segmented output image is shown in Fig. 25. Final segmentation results show that the proposed segmentation scheme must be significantly improved, especially in its contour detection stage, to provide results comparable with those of a human photointerpreter.

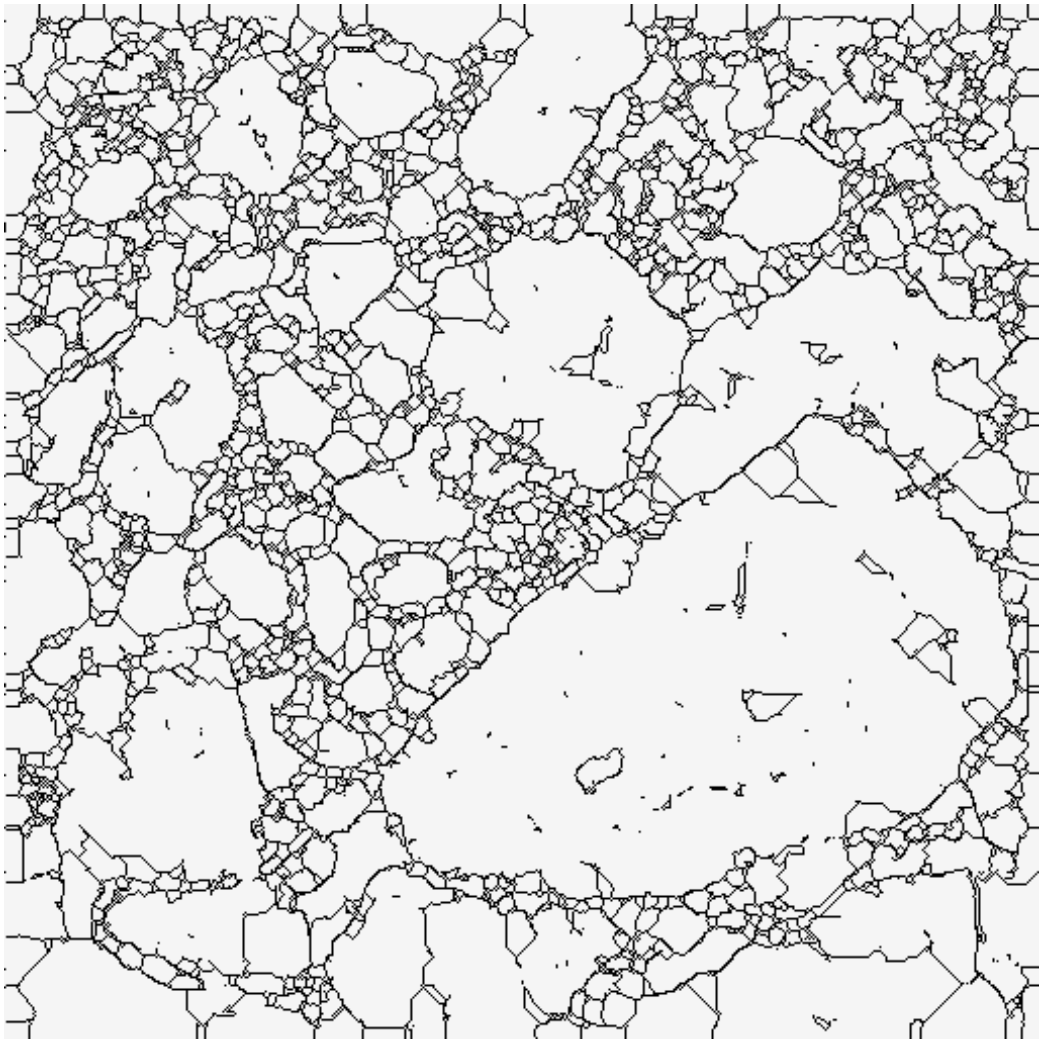

Figure 23: Final segment boundaries obtained by merging segments shown in Fig. 14.

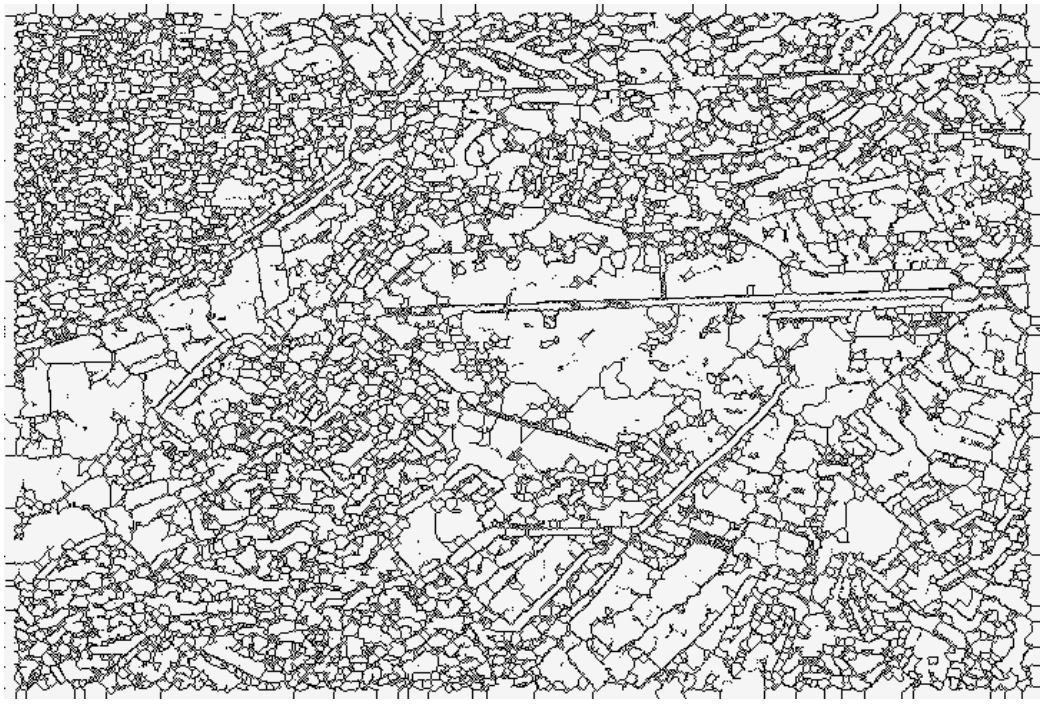

Figure 24: Final segment boundaries obtained by merging segments shown in Fig. 18.

7.1 Quantitative segmentation assessment

To compare quantitatively the SAR segmentation scheme proposed in this paper with other techniques found in the literature, it is important to stress that there is no single goal for picture partition algorithms [63], [64]. Therefore, a system developed to compare segmentation results must employ [63]: i) an entire set of measures of success (termed battery test) to account for the fuzziness of perceptual segmentation; and ii) a test set of images to allow exploitation of supervised data, i.e., of *a priori* knowledge about the objects in a scene, so that the external environment provides the generic (vague) segmentation task with an explicit goal. More efforts of the remote sensing community should be focused on the definition of a standard battery test and test set of images. Up to now, these authors have no expertise in developing a standard battery test and a set of test images [65], [66].

8 Conclusions

Our work started by observing that a standard SAR image segmentation procedure found in the literature provides output images that are oversegmented for classification tasks. This procedure is centered on a well-known speckle contour detector, termed CFAR, which employs: i) odd-symmetric filters as step edge detectors, working independently at (four) different spatial scales; ii) a competitive (coupling) mechanism among filters working at the same scale but featuring different orientation; and iii) a hierarchy of scale-dependent theoretical thresholds computed from background knowledge about speckled radiance. To

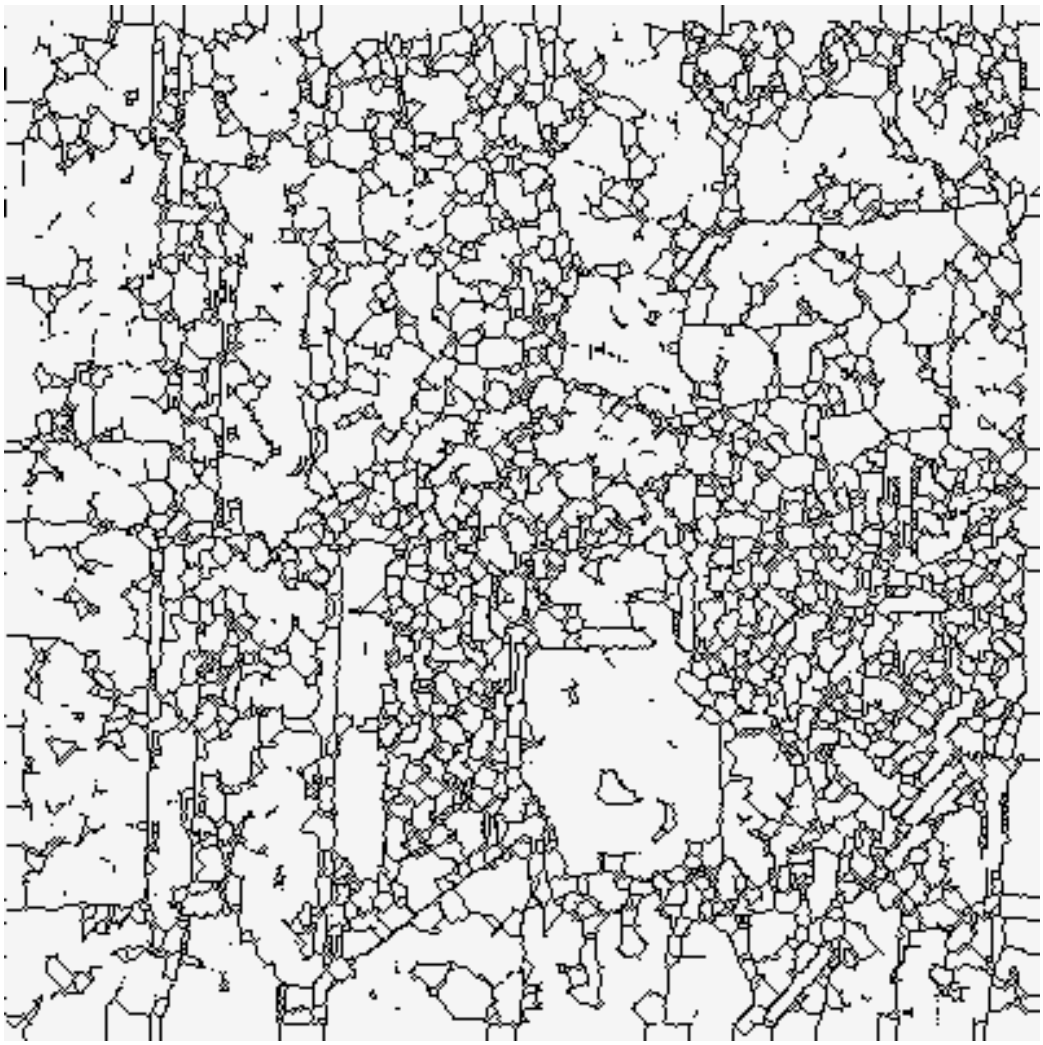

Figure 25: Final segment boundaries obtained by merging segments shown in Fig. 21.

reduce oversegmentation phenomena, an alternative SAR image segmentation scheme, exploiting four processing blocks taken from the literature, has been proposed. The core of this processing scheme is a speckle model-free contour detector, termed CACD, which employs: i) simple cells as odd- and even-symmetric filter pairs; ii) complex cells computing the Pythagorean sum of simple cell outputs; iii) a competitive (coupling) mechanism among complex cells featuring: a) different orientations, but the same size; and b) the same orientation, but different sizes; and iv) a user-defined threshold defined as a relative number. By changing its pair of resolution scales, CACD has shown abilities in detecting image structures (edges, ramps, ridges, roofs) as well as texture transitions. Unfortunately CACD does not provide a mechanism capable of effectively combining signals of complex cells working at (uo to four) different spatial scales. For example, CACD loses small/thin details in airborne SAR images while working at lower spatial resolutions.

Although inspired by the PVC module of the mammalian visual system, CACD is far from being "biologically plausible" both at microscopic and macroscopic (system) levels. From the macroscopic viewpoint, note that our basic idea of developing an artificial preattentive visual architecture as an independent image processing system is inconsistent with current knowledge of the mammalian visual system, for which there is evidence proving the existence of a feed-back loop between the preattentive and the attentive visual stages [67].

Our current implementation of the SAR segmentation scheme requires only one user-defined parameter to process different SAR images. This parameter is a contrast threshold provided with a clear physical meaning and belonging to the normalized range (0,1). Thus, the proposed segmentation scheme is easy to use.

The advantages of the CACD-based approach to SAR image segmentation are that: i) for classification purposes, it reduces oversegmentation phenomena affecting standard SAR image segmentation techniques based on CFAR; as a consequence, it also reduces processing time required to run region growing techniques employed in cascade to eliminate artifacts; ii) the same segmentation scheme can be employed to segment SAR images as well as monochromatic and multi-spectral incoherent imagery; and iii) multidisciplinary knowledge (stemming from neurophysiology, psychophysics, computer vision and image processing [44]) can be employed to improve the processing scheme.

The limitations of the CACD-based approach to SAR image segmentation are that: i) small/thin details are lost in airborne SAR images; ii) T- and X-junctions are poorly detected; and iii) region growing techniques are required to eliminate artifacts and reduce oversegmentation. Despite these drawbacks, our qualitative interpretation of experimental results is that the objective of developing a SAR segmentation process independent of background knowledge on the data source is feasible. This interpretation encourages further research focused on how low-level visual systems should combine responses of multi-scale filter banks for detecting image structures and texture transitions preattentively, i.e., at a single glance while no prior domain-specific knowledge about the data source and the content of the scene is employed.

Appendix

The basic scheme of CFAR is the following:

```
Input L = number of looks of the intensity SAR image;
for each increasing window size N_i, i = 1, ..., 4,
{
    compute ratio (similarity) threshold T_i(N_i, L);
    /* T_1 < .... < T_4, i.e., threshold becomes
    less restrictive as window size increases;
    moreover, T_i increases if L increases*/
}
for each pixel P
{
    Edge(P) = FALSE;
    for each window of increasing size i = 1, ..., 4,
    {
        for each orientation j=1,...,4,
        {
            compute ratio (similarity) value r_{i,j};
        }
        r_i = arg min_{j=1,...,4} {r_{i,j}};
        if(r_i < T_i)
        {
            Edge(P) = TRUE;
            break;
            /* skip iterations on window size */
        }
    }
}
```

References

[1] R. C. Jain and T. O. Binford, "Ignorance, myopia and naivetè in computer vision systems," *Comput., Vision, Graphics, Image Processing: Image Understanding*, vol. 53, pp. 112-117, 1991.

[2] M. Kunt, Comments on "Dialogue", a series of articles generated by the paper entitled "Ignorance, myopia and naivetè in computer vision systems," *Comput., Vision, Graphics, Image Processing: Image Understanding*, vol. 54, pp. 428-429, 1991.

[3] T. Pavlidis, "Why progress in machine vision is so slow," *Pattern Recognition Letters*, vol. 13, pp. 221-225, 1992.

[4] P. Zamperoni, "Plus ça va, moins ça va," *Pattern Recognition Letters*, vol. 17, no. 7, pp. 671-677, June 1996.

[5] E. Nezry, A. Lopes, D. Ducrot-Gambart, C. Nezry and J.S. Lee, "Supervised classification of K-distributed SAR images of natural targets and probability

of error estimation," *IEEE Trans. Geosci. Remote Sensing*, vol. 34, no. 5, pp. 1233-1242, 1996.

[6] H. Skriver, *Extraction of Sea Ice Parameters from Synthetic Radar Images*, Ph.D. Thesis, Technical University of Denmark, 1989.

[7] Y. Sun, A. Carlström and J.Askne, "SAR image classification of ice in the gulf of Bothnia," *Int. J. Remote Sensing*, vol. 13, no. 13, pp. 2489-2514, 1992.

[8] M. E. Shokr, "Evaluation of second-order texture parameters for sea ice classification from radar images," *J. of Geophysical Research*, vol. 96, no. 6, pp. 10.625-10.640, June, 1991.

[9] A. Sephton, L. Brown, J. Macklin, K. Partington and J. Veck, "Segmentation of synthetic aperture radar images of sea ice," *Int. J. Remote Sensing*, vol. 15, no. 4, pp. 803-825, 1994.

[10] R. G. Caves, S. Quegan, and R. G. White, "The use of segmentation for change detection in spaceborne SAR images," *Proc. of the 19th Annual Conference of the Remote Sensing Society: Towards Operational Applications*, ed. K. Hilton, Nottingham: Remote Sensing Society, pp. 168-175, 1993.

[11] E. Nezry, A. Lopes, and F. Yakam-Simen, "Prior scene knowledge for the Bayesian restoration of mono- and multi-channel SAR images," *Proc. IGARSS '97.*

[12] P. C. Smits, and S. G. Dellepiane, "Synthetic aperture radar image segmentation by a detail preserving Markov Random Field approach," *IEEE Trans. Geosci. Remote Sensing*, vol. 35, no. 4, pp. 844-857, 1997.

[13] A. Lopes, R. Touzi and E. Nezry, "Adaptive speckle filters and scene heterogeneity," *IEEE Trans. Geosci. Remote Sensing*, vol. 28, no. 6, pp. 992-1000, Nov. 1990.

[14] E. Nezry, A. Lopes and R. Touzi, "Detection of structural and textural features for SAR images filtering," *Proc. IGARSS '91*, vol. 3, pp. 2169-2172.

[15] A. Lopes, E. Nezry, R. Touzi and H. Laur, "Structure detection and statistical adaptive speckle filtering in SAR images," *Int. J. Remote Sensing*, vol. 14, no. 9, pp. 1735-1758, 1993.

[16] A. Lopes, E. Nezry, R. Touzi and H. Laur, "Maximum *a posteriori* speckle filtering and first order texture models in SAR images," *Proc. IGARSS '90*, College Park, MD, May 1990, vol. 3, pp. 2409-2412.

[17] E. Nezry, M. Leysen and G. De Grandi, "Speckle and scene spatial estimators for SAR image filtering and texture analysis: some applications to agriculture, forestry, and point targets detection," *Proc. SPIE-EUROPTO: SAR Data Processing for Remote Sensing*, Paris, France, Sept. 1995, vol. 2584, pp. 110-120.

[18] F. T. Ulaby, F. Kouyate, B. Brisco and T. H. Lee Williams, "Textural information in SAR images," *IEEE Trans. Geosci. Remote Sensing* , vol. 24, no. 2, pp. 235-245, March 1986.

[19] D. Smith, "Speckle reduction and segmentation of synthetic aperture radar images," *Int. J. Remote Sensing*, vol. 17, no. 11, pp. 2043-2057, 1996.

[20] J. Lee and I. Jurkevich, "Segmentation of SAR images," *IEEE Trans. Geosci. Remote Sensing*, vol. 27, pp. 674-680, 1989.

[21] M. Tur, K. C. Chin and J. W. Goodman, "When is speckle multiplicative?", *Appl. Opt.*, vol. 21, no. 7, pp. 1157-1159, April 1982.

[22] J. Lee,"Refined filtering of image noise using local statistics," *Computer Graphics and Image Processing*, vol. 15, pp. 380-389, 1981.

[23] D. Kuan, A. Sawchuk, T. Strand and P. Chavel, "Adaptive restoration of images with speckle," *IEEE Trans. Acoustics, Speech, and Signal Processing*, vol. ASSP-35, no. 3, pp. 373-383, March 1987.

[24] A. Baraldi and F. Parmiggiani, "A refined Gamma MAP SAR speckle filter with improved geometrical adaptivity," *IEEE Trans. Geosci. Remote Sensing*, vol. 33, no. 5, pp. 1245-1257, Sept. 1995.

[25] A. Lopes, R. Touzi and E. Nezry, "Adaptive speckle filters and scene heterogeneity," *IEEE Trans. Geosci. Remote Sensing* , vol. 28, no. 6, pp. 992-1000, Nov. 1990.

[26] E. Nezry, H. Kohl and H. De Groof, "Restoration and enhancement of textural properties in SAR images using second order statistics," *Proc. SPIE-EUROPTO: SAR Data Processing for Remote Sensing*, Rome, Italy, Sept. 1994, vol. 2316, pp. 115-124.

[27] R. Fjørtoft, F. Lebon, F. Sery, A. Lopes, P. Marthon, E. Cubero Castan, "A region-based approach to the estimation of local statistics in adaptive speckle filters," *Proc. IGARSS '96*, vol. 1, pp. 457-459.

[28] R. Touzi, A. Lopes and P. Bousquet,"A statistical and geometrical edge detector for SAR images," *IEEE Trans. Geosci. Remote Sensing*, vol. 26, no. 6, pp. 764-773, Nov. 1988.

[29] W. T. Freeman, *Steerable Filters and Local Analysis of Image Structures*, Ph. D. Thesis, Massachusetts Institute of Technology, 1992.

[30] P. Perona, "Steerable-scalable kernels for edge detection and junction analysis," *Proc. European Conference on Computer Vision*, pp. 3-18, 1992.

[31] V. Torre and T. Poggio, "On edge detection," *IEEE Trans. Pattern Analysis Machine Intel.*, vol. 8, no. 2, pp. 147-163, 1986.

[32] D. Marr, *Vision*, New York: Freeman, 1982.

[33] E. R. Kandel, "Perception of motion, depth and form", in *Principles of Neural Science*, E. Kandel and J. Schwartz, Eds., Norwalk, CT: Appleton and Lange, 1991, pp. 441-466.

[34] P. Gouras, "Cortical mechanisms of colour vision", in *The Perception of Colour*, Vol. 6: *Vision and Visual Dysfunction*, P. Gouras, Ed., CRC Press, Boca Raton, FL, 1991, pp. 179-197.

[35] A. P. Dhawan and T. Dufresne, "Neural model-based approach to image enhancement," *Optical Engineering*, vol. 33, no. 4, pp. 1156-1165, 1994.

[36] I. Fogel and D. Sagi, "Gabor filters as texture discriminator," *Biol. Cybern.*, vol. 61, pp. 103-113, 1989.

[37] C. Mason and E. R. Kandel, "Central visual pathways", in *Principles of Neural Science*, E. Kandel and J. Schwartz, Eds., Norwalk, CT: Appleton and Lange, 1991, pp. 420-439.

[38] P. Gouras, "Color vision", in *Principles of Neural Science*, E. Kandel and J. Schwartz, Eds., Norwalk, CT: Appleton and Lange, 1991, pp. 467-479.

[39] H. R. Wilson and J. R. Bergen, "A four mechanism model for threshold spatial vision," *Vision Res.*, vol. 19, pp. 19-32, 1979.

[40] D. C. Burr and M. C. Morrone, "A nonlinear model of feature detection", in *Nonlinear Vision: Determination of Neural Receptive Fields, Functions, and Networks*, R. B. Pinter and N. Bahram, Eds., Boca Raton: CRC Press, 1992, pp. 309-327.

[41] J. Jones and L. Palmer, "An evaluation of the two-dimensional Gabor filter model of simple receptive fields in cat striate cortex," *J. Neurophysiol.*, vol. 58, pp. 1233-1258, 1987.

[42] A. Baraldi and F. Parmiggiani, "Combined detection of intensity and chromatic contours in color images," *Optical Engineering*, vol. 35, no. 5, pp. 1413-1439, May 1996.

[43] M. Tessier-Lavigne, "Phototrasduction and information processing in the retina," in *Principles of Neural Science*, E. Kandel and J. Schwartz, Eds., Norwalk, CT: Appleton and Lange, 1991, pp. 401-418.

[44] R. Serra and G. Zanarini, *Complex systems and cognitive processes*, Berlin: Springer-Verlag, 1990.

[45] H. Derin and H. Elliott, "Modeling and segmentation of noisy and textured images using Gibbs random fields," *IEEE Trans. Patt. Anal. Machine Intelligence*, vol. PAMI-9, no. 1, pp. 39-55, 1987.

[46] T. N. Pappas, "An adaptive clustering algorithm for image segmentation," *IEEE Trans. on Signal Processing*, vol. 40, no. 4, pp. 901-914, 1992.

[47] J. Canny, "A computational approach to edge detection", *IEEE Trans. Pattern Analysis Machine Intel.*, vol. PAMI-8, no. 6, pp. 679-698, 1986.

[48] D. Dunn, W. E. Higgins and J. Wakeley, "Texture segmentation using 2-D Gabor elementary functions," *IEEE Trans. Pattern Analysis Machine Intel.* vol. 16, no. 2, pp. 130-149, 1994.

[49] M. C. Morrone and R. Owens, "Feature detection from local energy," *Pattern Rec. Lett.*, vol. 1, pp. 103-113, 1987.

[50] J. Malik and P. Perona, "Preattentive texture discrimination with early vision mechanisms," *J. Opt. Soc. Am. A*, vol. 7, no. 5, pp. 923-932, 1990.

[51] I. Fogel and D. Sagi, "Gabor filters as texture discriminator," *Biol. Cybern.*, vol. 61, pp. 103-113, 1989.

[52] J. Tilton, "Image segmentation by iterative parallel region growing and splitting," *Proc. IGARSS '89*, Vancouver, BC, Canada, July 1989, pp. 2420-2423.

[53] A. Baraldi and F. Parmiggiani, "Segmentation driven by an iterative pairwise mutually best merge criterion," *Proc. IGARSS '95*, Firenze, Italy, July 1995, vol. 1, pp. 89-92.

[54] A. Baraldi and F. Parmiggiani, "A region growing algorithm to detect segments featuring low contrast in multispectral images," *Proc. EOS-SPIE: Image and Signal Processing for Remote Sensing II*, Paris, France, Sept. 1995, vol. 2579, pp. 234-247.

[55] J. Le Moigne and J. Tilton, "Refining image segmentation by integration of edge and region data," *IEEE Trans. Geosci. Remote Sensing*, vol. 33, no. 3, pp. 605-615, May 1995.

[56] J. Beaulieu and M. Goldberg, "Hierarchy in picture segmentation: a stepwise optimization approach," *IEEE Trans. Pattern Anal. Machine Intell.*, vol. 11, no. 2, pp. 150-163, Feb. 1989.

[57] R. M. Haralick, "Statistical and structural approaches to texture," *Proc. of the IEEE*, vol. 67, no. 5, pp. 786-804, 1979.

[58] A. Baraldi and F. Parmiggiani, "An investigation of textural characteristics associated with gray level cooccurence matrix statistical parameters," *IEEE Trans. Geosci. Remote Sensing*, vol. 33, no. 2, pp. 293-304, March 1995.

[59] J. I. Yellott, "Implications of triple correlation uniqueness for texture statistics and the Julesz conjecture," *J. Opt. Soc. Am. A*, vol. 10, no. 5, pp. 777-793, 1993.

[60] R. M. Haralick and L. G. Shapiro, "Survey: image segmentation techniques," *Computer Vision, Graphics, and Image Process.*, vol. 29, pp. 100-132, 1985.

[61] A. Baraldi and F. Parmiggiani, "A neural network for unsupervised categorization of multivalued input patterns: an application to satellite image clustering," *IEEE Trans. Geosci. Remote Sensing*, vol. 33, no. 2, pp. 305-316, March 1995.

[62] A. Baraldi and E. Alpaydın, "Simplified ART: A new class of ART algorithms," International Computer Science Institute, Berkeley, CA, TR-98-004.

[63] L. Delves, R. Wilkinson, C. Oliver and R. White, "Comparing the performance of SAR image segmentation algorithms," *Int. J. Remote Sensing*, vol. 13, no. 11, pp. 2121-2149, 1992.

[64] J. P. Coquerez, S. Phillip and R. Zeboudi, "Comparaison de mèthodes de segmentation d'images," *Proc. 15th GRETSI Symposium*, Juan-les-Pins, France, Sept. 1995, pp. 1355-1360.

[65] A. Hoover, G. Jean-Baptiste, X. Jiang, P. J. Flynn, H. Bunke, D. G. Goldgof, K. Bowyer, D. W. Eggert, A. Fitzgibbon, and R. B. Fisher, "An experimental comparison of range image segmentation algorithms," *IEEE Trans. Patt. Anal. Machine Intelligence*, vol. 18, no. 7, pp. 673-688, 1996.

[66] M. Heath, S. Sarkar, T. Sanocki, and K. Bowyer, "Comparison of edge detectors: A methodology and initial study," *Computer Vision and Pattern Recognition '96*, San Francisco, CA, June 1996.

[67] S. M. Kosslyn, W. L. Thompson, I. J. Kim and N. M. Alpert, "Topographical representations of mental images in primary visual cortex," *Nature*, vol. 378, pp. 496-497, 1995.